Structure-Property Relationship Studies for High-Performance Organic Field-Effect Transistors and Flexible Photosensors

Jayeon Hong

Department of Energy Engineering

Graduate school of UNIST

2015

Structure-Property Relationship Studies for High-Performance Organic Field-Effect Transistors and Flexible Photosensors

Jayeon Hong

Department of Energy Engineering

Graduate school of UNIST

Structure-Property Relationship Studies for High-Performance Organic Field-Effect Transistors and Flexible Photosensors

A thesis

submitted to the Graduate School of UNIST

in partial fulfillment of the

requirements for the degree of

Master of Science

Jayeon Hong

12. 19. 2014

Approved by

Advisor

Byeong-Su Kim

Structure-Property Relationship Studies for High-Performance Organic Field-Effect Transistors and Flexible Photosensors

Jayeon Hong

This certifies that the thesis of Jayeon Hong is approved.

12. 19. 2014

Signature

Advisor: Byeong-Su Kim

Signature

Joon Hak Oh: Thesis Committee Member #1

Signature

Changduk Yang: Thesis Committee Member #2

Abstract

Recently, organic field-effect transistors (OFETs) and OFET-based sensors have attracted great interest for their potential for use in low-cost, large-area, lightweight, flexible, and wearable electronic devices. Various researches for high-performance OFET devices have been reported to achieve high mobility, air stability, and flexibility through molecular design and optimized device configuration. In addition, OFET-based sensors based on various flexible substrates and nanostructured organic semiconducting materials have been studied for use in wearable sensor devices with high sensitivity and excellent mechanical stability under severely bent condition.

In **chapter 1**, we studied the relationship between molecular structure in a film state and electrical performance of OFET devices. We fabricated high-performance *n*-channel OFETs based on semiconducting copolymers containing strong electron-withdrawing unit, naphthalene diimide (NDI). NDI-based copolymers with various donor moieties, acene- (benzene (Bz), naphthalene (Np), and pyrene (Py)) and heteroacene-type components (selenophene (Se) and thiophene (Th)) were designed to enhance efficient intramolecular charge transfer (ICT). The OFET performance of NDI-based copolymers was optimized in bottom-gate top-contact (BGTC) device configuration by tuning the solution-deposition methods and thermal annealing at various temperatures. The electrical characteristics of the devices fabricated with **PNDI-Np**, acene-based centrosymmetric copolymer, showed the best electron mobility of 5.63×10^{-2} $cm^2V^{-1}s^{-1}$ among the developed polymers including axisymmetric copolymers with electron-rich donor groups. This result reveals the stronger influence of the geometric feature on the OFET performance rather than electron-donating strength of the donors in the molecular backbone.

In **chapter 2**, we report on highly flexible OFET-based photosensors based on a textile substrate and organic semiconducting nanofibers. Textile-based OFET devices with bottom-gate bottom-contact (BGBC) configuration consist of poly(ethylene terephthalate) (PET) textile substrate buffered with polydimethylsiloxane (PDMS), gate electrode, PDMS dielectric layer and source-drain electrode. Electrospun organic semiconducting nanofibers based on a *p*-type semiconducting polymer, poly(3,3‴-didodecylquarterthiophene) (PQT-12) were used as the active layer. The field-effect mobility of textile-based OFETs was as high as 2.96×10^{-3} $cm^2V^{-1}s^{-1}$ in N_2 atmosphere. Under the bending test with extremely low bending radius of 0.75 mm, the device performance showed superior mechanical stability compared with the PET film-type substrates or PDMS-only substrates. Furthermore, they exhibited highly stable electrical characteristics after ~1000 cycles of bending test. The electrical responses of textile-based OFETs with photo-responsive organic semiconducting nanofibers were also investigated under the irradiation of light with various wavelengths. The developed method may pave a viable way for the fabrication of wearable photosensing or photoswitching devices.

Contents

List of Figures ---------- 5

List of Tables ---------- 8

Introduction of Organic Field-Effect Transistors (OFETs)

I. Basics of OFETs ---------- 10

II. References ---------- 13

Chapter 1. Comparison of Structural Features and Electron-Donating Strength of Co-Units in Naphthalene Diimide (NDI)-based Copolymers for High-Performance Organic Field-Effect Transistors

I. Introduction ---------- 16

II. Experimental ---------- 18

2.1 Fabrication of NDI-based OFETs ---------- 18

2.2 Characterization of NDI-based OFETs ---------- 18

III. Results and Discussion ---------- 19

3.1 Characterization of optical and electrochemical properties, and DFT calculation ------- 19

3.2 Thin Film Morphology Analyses ---------- 23

3.3 Electrical Characteristics of NDI-based OFETs ---------- 26

IV. Conclusion ---------- 29

V. References ---------- 30

Chapter 2. Textile-Based Organic Field-Effect Transistors and Application to Wearable Photosensors with High Flexibility and Mechanical Stability

I. Introduction ---------- 36

II. Experimental ---------- 37

2.1 Preparation of textile-based OFET substrate ---------- 37

2.2 Fabrication of PQT-12:PEO nanofibers ---------- 37

2.3 Characterization of textile-based OFET devices ---------- 38

III. Result and Discussion ---------- 40

3.1 Fabrication of PET-textile OFETs ---------- 40

3.2 Electrical characteristics of textile-based OFETs ---------- 44

3.3 Mechanical Stability ---------- 46

3.4 Optoelectronic characteristics ---------- 51

3.5 Photosensor application ---------- 54

IV. Conclusion ---------- 57

V. References ---------- 58

Acknowledgements ---------- 61

List of Figures

Figure 1. The typical structure of conventional unipolar OFETs.

Figure 2. Current-voltage (*I-V*) characteristics of OFETs: (a) output characteristics, (b) transfer characteristics in the linear regime, (c) transfer characteristics in the saturation regime.

Figure 3. Schematic diagrams of structural configuration of OFETs: bottom-gate bottom-contact (BGBC), bottom-gate top-contact (BGTC), top-gate bottom-contact (TGBC), and top-gate top-contact (TGTC).

Chapter 1.

Scheme 1.1. Molecular structures of NDI-based D-A copolymers

Figure 1.1. Normalized UV-Vis absorption spectra of NDI-based D-A copolymers in (a) chloroform solution and (b) as thin solid films.

Figure 1.2. (a) Cyclic voltammograms of NDI-based D-A copolymers in thin films drop-cast on a platinum working electrode and tested in n-Bu4NPF6/CH3CN solution (scan rate, 50 mVs-1). (b) Calculated molecular orbitals and optimized geometry for the model dimers of NDI-based copolymers, respectively (B3LYP/6-31G*). (1) and (2) are used to symbolize the NDI acceptor and donor portions, respectively, for clarity of either staggered or eclipsed conformation. The side chains were replaced with methyl groups to simplify the calculation.

Figure 1.3. Out-of-plane X-ray diffraction (XRD) patterns of the annealed NDI copolymer thin films that show the best n-channel performance.

Figure 1.4. AFM height images of (a) **PNDI-Bz**, (b) **PNDI-Np**, (c) **PNDI-Py**, (d) **PNDI-Th**, (e) **PNDI-Se** polymer films annealed at temperatures for the best n-channel performance. Scale bar = 1 μm.

Figure 1.5. (a) Schematic illustration of OFET in BGTC structure. (b) Optimized n-channel transfer characteristics of OFETs based on annealed NDI copolymer thin films. (c) Output characteristics of the best-performing n-channel **PNDI-Np** OFET annealed at 150 ℃.

Figure S1.1. Out-of-plane X-ray diffraction (XRD) patterns of the as-cast NDI copolymer thin films.

Figure S1.2. AFM height images of (a) **PNDI-Bz**, (b) **PNDI-Np**, (c) **PNDI-Py**, (d) **PNDI-Se**, (e) **PNDI-Th** as-cast films. Scale bar = 1 μm.

Figure S1.3. Transfer curves of OFETs based on the as-cast NDI copolymer films.

Figure S1.4. Transfer characteristics of (a) **PNDI-Py** annealed at 120 ℃, (b) **PNDI-Th** and (b) **PNDI-Se** annealed at 220 ℃ at hole-enhancement operation.

Chapter 2.

Scheme 2.1. Molecular structure of poly(3,3‴-didodecylquarterthiophene) (PQT-12) and poly(ethylene oxide) (PEO)

Figure 2.1. Schematic diagram of electrospinning process.

Figure 2.2. OM image of pristine PET textile (x100)

Figure 2.3. The fabrication process of textile-based OFETs.

Figure 2.4. Cross-sectional SEM image of textile-based OFETs

Figure 2.5. OM images of PQT-12:PEO NFs on bright-field (left, above) and dark-field (left, below), and SEM image of PQT-12:PEO NFs (right).

Figure 2.6. Electrical characteristics of textile-based OFETs; a) Transfer and b) Output characteristics.

Figure 2.7. Typical photographic image of textile-based OFET upon bending at radius of 0.75 mm.

Figure 2.8. a) Transfer characteristics under different bending radii (6.7, 4.6, 3.5, 2.7, 1.6, 0.75 mm) and b) change in on-current and off-current under various bending radius.

Figure 2.9. Photographic image of textile-based OFET upon bending cycle test.

Figure 2.10. a) Transfer characteristics and b) change in on-current and off-current upon bending cycle test (up to 1000 cycles) with bending radius of 2.5 mm.

Figure 2.11. Comparison of change in on-current under various bending radii with OFETs based on PET film substrate and PDMS-only substrate

Figure 2.12. UV–vis spectra of PQT-only, PQT-12:PEO solution in chlorobenzene and spin-coated PQT-only, PQT-12:PEO thin-film, and PQT-12:PEO NFs.

Figure 2.13. Transfer characteristics of textile-based OFETs under different light source.

Figure 2.14. Real-time photo-sensing graph under 470 nm (blue) and 670 nm (red).

Figure 2.15. a) Photographic image of photosensing matrix (10×10) of the textile-based OFETs, and b) schematic illustration of sensor arrays partially exposed to the external light source. (intensity = 6 mW cm^{-2}) c) Spatial photosensing map of the textile-based photosensor matrix. The polychromatic light was

positioned on (2, 1) of the matrix.

Figure S2.1. a) Transfer and b) Output characteristics of PQT-12:PEO nanofibers on OTS-treated SiO2 (300 nm)/n-doped Si wafer with BGBC geometry.

Figure S2.2. a) Transfer and b) Output characteristics of PQT-12:PEO nanofibers on coplanar-gate transistor based on ion-gel dielectric and polyimide (PI) substrate.

List of Tables

Chapter 1.

Table 1.1. Optical and electrochemical properties of NDI-based D-A copolymers.

Table 1.2. Peak assignments for the out-of-plane XRD patterns of as-cast and annealed NDI-based polymer films.

Table 1.3. *I-V* characteristics of NDI-based copolymer OFETs obtained at different annealing temperatures.

Chapter 2.

Table 2.1. Summary of relative decrease of on current (%) of PET textile, PET film, and PDMS-only substrate under different bending radius.

Table 2.2. Summary of maximum absorption wavelength (λ_{max}) of PQT-12-only, PQT-12+PEO solution in chlorobenzene, spin-coated PQT-12-only, PQT-12+PEO thin-film, PQT-12:PEO single nanofibers

Introduction of Organic Field-Effect Transistors (OFETs)

I. Basics of OFETs

In the recent decades, there has been great attention in the electronic devices based on organic semiconductors such as organic field-effect transistors (OFETs)[1], organic solar cells (OSCs)[2], and organic light-emitting diodes (OLEDs)[3] due to their advantages of low cost, light weight, solution-processability, and flexibility. In particular, OFETs are the strong candidate for use in next-generation electronic devices such as flexible displays, electronic papers, wearable sensor devices, electronic skins, etc.[4]

The typical structure with working principle and electrical characteristics of OFETs are described in Figure 1 and 2, respectively.[5,6] Field-effect transistors (FETs) developed as switching and amplifying devices have three-terminal systems consisting of gate electrode and source/drain electrodes. The source/drain electrodes contact directly with semiconductor layer which is separated with gate electrode by gate dielectric layer.[5] Figure 3 shows the four types of device structures for OFETs according to the location of gate electrode and source/drain electrode. As the gate voltage (V_{GS}) is applied, the charge transporting channel is induced at the interface of the dielectric and semiconductor, therefore source-drain current (I_{DS}) can be increased by the potential difference between source and drain electrodes (V_{DS}).[7]

The OFET device performance is demonstrated by the three important parameters, the mobility (μ), the on/off ratio (I_{on}/I_{off}), the threshold voltage (V_{th}).[8] μ can be described as the charge carrier drift velocity per unit applied electric field. I_{on}/I_{off} is the ratio between on-current and off-current and V_{th} is the gate voltage when the charge transport channel is formed.[9] The mobility can be extracted from the following equations:

$$I_{DS} = \mu C_i W/L(V_{GS}\text{-}V_{th}\text{-}V_{DS}/2)V_{DS} \quad (V_{DS} < V_{GS} - V_{th}, \text{ linear regime})$$

$$I_{DS} = \mu C_i W/2L(V_{GS}\text{-}V_{th})^2 \quad (V_{DS} > V_{GS} - V_{th}, \text{ saturation regime})$$

where C_i is the capacitance of the gate dielectric, and W and L are channel width and length, respectively.

Depending on the kinds of charge carriers, there are two operation types of unipolar semiconductors, *p*-channel (hole) and *n*-channel (electron). We can also consider the ambipolar operation of semiconductors when both the hole and the electron can be used as the charge carriers in a semiconducting layer.[10] When the large electric field is applied by negative/positive V_{GS}, the HOMO and LUMO levels of organic semiconductors shift up/down to Fermi levels of the metal contact, causing hole/electron to move through HOMO/LUMO in the channels from the source/drain electrodes.[11]

To realize OFETs in practical electronic devices, their electrical performance and operation stability should be more improved. Tremendous efforts to develop the high-performance OFETs with

operational stability have been reported over the past decades[1] since the initial field-effect mobility of polythiophene was reported in 1980s[12]. Subsequently, the various molecular designs of organic semiconductors including small molecules, oligomers, and polymers have been introduced and applied to the devices to produce novel high-performance OFETs.[1] In the view of fabrication process, device configuration, introduction of self-assembled monolayer[13], change of device configuration with various dielectric[14] and electrode materials[15], deposition method of semiconducting materials[16] can significantly affect the electrical performance of OFET devices. As a result, the mobility of OFETs based on organic semiconductors reached over ~1 $cm^2V^{-1}s^{-1}$ of amorphous silicon. Recently, the hole and electron mobility was reported as over 40 $cm^2V^{-1}s^{-1}$ and 11 $cm^2V^{-1}s^{-1}$, respectively.[17,18]

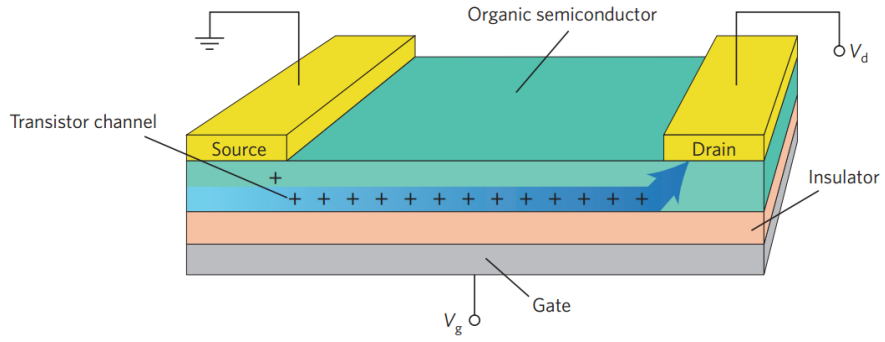

Figure 1. The typical structure of conventional unipolar OFETs.

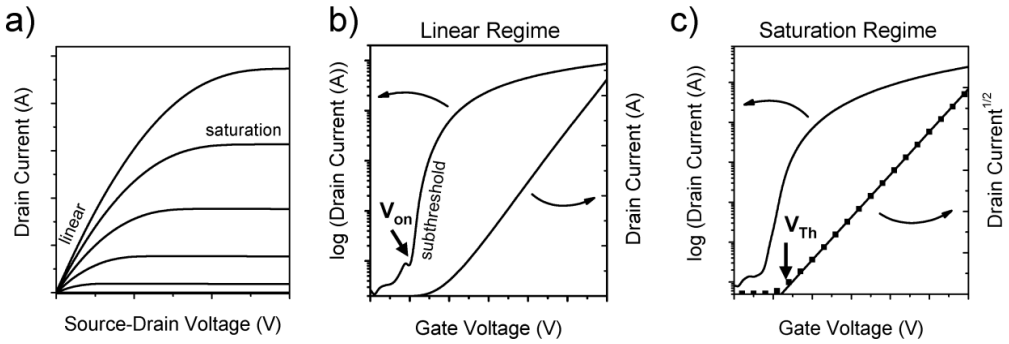

Figure 2. Current-voltage (*I-V*) characteristics of OFETs: (a) output characteristics, (b) transfer characteristics in the linear regime, (c) transfer characteristics in the saturation regime.

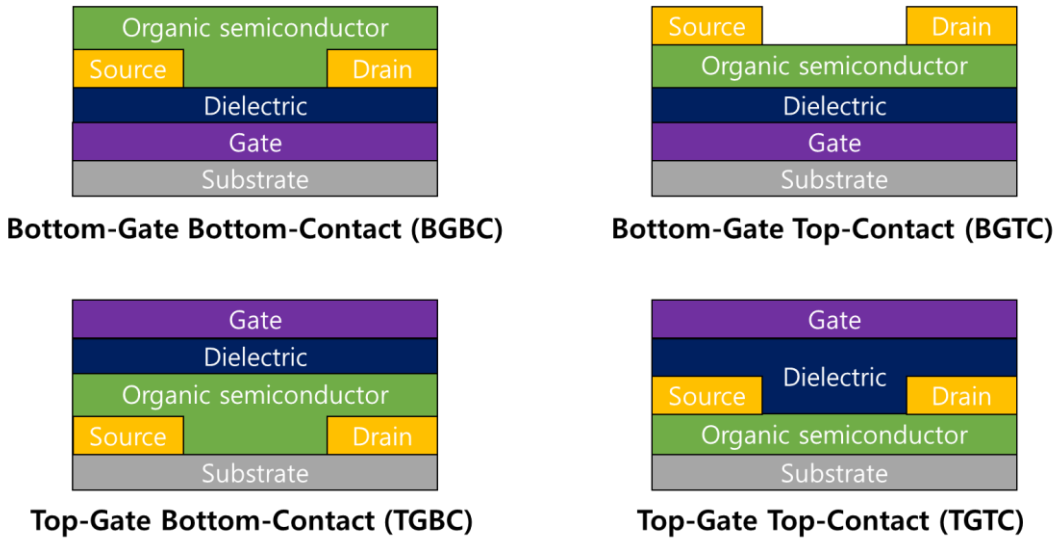

Figure 3. Schematic diagrams of structural configuration of OFETs: bottom-gate bottom-contact (BGBC), bottom-gate top-contact (BGTC), top-gate bottom-contact (TGBC), and top-gate top-contact (TGTC).

II. References

1. (a) Dong, H.; Fu, X.; Liu, J.; Wang, Z.; Hu, W., 25th Anniversary Article: Key Points for High-Mobility Organic Field-Effect Transistors. *Advanced Materials* **2013,** *25* (43), 6158-6183; (b) Sirringhaus, H., 25th Anniversary Article: Organic Field-Effect Transistors: The Path Beyond Amorphous Silicon. *Advanced Materials* **2014,** *26* (9), 1319-1335.

2. Heeger, A. J., 25th Anniversary Article: Bulk Heterojunction Solar Cells: Understanding the Mechanism of Operation. *Advanced Materials* **2014,** *26* (1), 10-28.

3. Kuik, M.; Wetzelaer, G.-J. A. H.; Nicolai, H. T.; Craciun, N. I.; De Leeuw, D. M.; Blom, P. W. M., 25th Anniversary Article: Charge Transport and Recombination in Polymer Light-Emitting Diodes. *Advanced Materials* **2014,** *26* (4), 512-531.

4. Wu, W.; Liu, Y.; Zhu, D., [small pi]-Conjugated molecules with fused rings for organic field-effect transistors: design, synthesis and applications. *Chemical Society Reviews* **2010,** *39* (5), 1489-1502.

5. Melzer, C.; von Seggern, H., Organic electronics: Enlightened organic transistors. *Nat Mater* **2010,** *9* (6), 470-472.

6. Zaumseil, J.; Sirringhaus, H., Electron and Ambipolar Transport in Organic Field-Effect Transistors. *Chemical Reviews* **2007,** *107* (4), 1296-1323.

7. Sirringhaus, H., Device Physics of Solution-Processed Organic Field-Effect Transistors. *Advanced Materials* **2005,** *17* (20), 2411-2425.

8. Park, J.; Park, K.-S.; Jeong, Y.-S.; Baek, K.-H.; Lee, B. K.; Kim, D.-P.; Ryu, J.-H.; Do, L.-M.; Imamura, H.; Yase, K.; Choi, J. S., Characteristic Variations of Graphene Field-Effect Transistors Induced by CF 4 Gas. *Japanese Journal of Applied Physics* **2012,** *51* (8R), 081301.

9. Yamashita, Y., Organic semiconductors for organic field-effect transistors. *Science and Technology of Advanced Materials* **2009,** *10* (2), 024313.

10. Chen, Z.; Lee, M. J.; Shahid Ashraf, R.; Gu, Y.; Albert-Seifried, S.; Meedom Nielsen, M.; Schroeder, B.; Anthopoulos, T. D.; Heeney, M.; McCulloch, I.; Sirringhaus, H., High-Performance Ambipolar Diketopyrrolopyrrole-Thieno[3,2-b]thiophene Copolymer Field-Effect Transistors with Balanced Hole and Electron Mobilities. *Advanced Materials* **2012,** *24* (5), 647-652.

11. Rivnay, J.; Mannsfeld, S. C. B.; Miller, C. E.; Salleo, A.; Toney, M. F., Quantitative Determination of Organic Semiconductor Microstructure from the Molecular to Device Scale. *Chemical Reviews* **2012,** *112* (10), 5488-5519.

12. Tsumura, A.; Koezuka, H.; Ando, T., Macromolecular electronic device: Field-effect transistor with a polythiophene thin film. *Applied Physics Letters* **1986,** *49* (18), 1210-1212.

13. Miozzo, L.; Yassar, A.; Horowitz, G., Surface engineering for high performance organic electronic devices: the chemical approach. *Journal of Materials Chemistry* **2010,** *20* (13), 2513-2538.

14. Veres, J.; Ogier, S.; Lloyd, G.; de Leeuw, D., Gate Insulators in Organic Field-Effect Transistors. *Chemistry of Materials* **2004,** *16* (23), 4543-4555.

15. (a) Li, L.; Meise-Gresch, K.; Jiang, L.; Du, C.; Wang, W.; Fuchs, H.; Chi, L., The Electrode's Effect on the Stability of Organic Transistors and Circuits. *Advanced Materials* **2012,** *24* (22), 3053-3058; (b) Li, L.; Jiang, L.; Wang, W.; Du, C.; Fuchs, H.; Hu, W.; Chi, L., High-Performance and Stable Organic Transistors and Circuits with Patterned Polypyrrole Electrodes. *Advanced Materials* **2012,** *24* (16), 2159-2164; (c) Hong, J.-P.; Park, A.-Y.; Lee, S.; Kang, J.; Shin, N.; Yoon, D. Y., Tuning of Ag work functions by self-assembled monolayers of aromatic thiols for an efficient hole injection for solution processed triisopropylsilylethynyl pentacene organic thin film transistors. *Applied Physics Letters* **2008,** *92* (14), -; (d) Hamadani, B. H.; Corley, D. A.; Ciszek, J. W.; Tour, J. M.; Natelson, D., Controlling Charge Injection in Organic Field-Effect Transistors Using Self-Assembled Monolayers. *Nano Letters* **2006,** *6* (6), 1303-1306.

16. (a) Lee, J.; Han, A. R.; Yu, H.; Shin, T. J.; Yang, C.; Oh, J. H., Boosting the Ambipolar Performance of Solution-Processable Polymer Semiconductors via Hybrid Side-Chain Engineering. *Journal of the American Chemical Society* **2013,** *135* (25), 9540-9547; (b) Kang, B.; Lee, W. H.; Cho, K., Recent Advances in Organic Transistor Printing Processes. *ACS Applied Materials & Interfaces* **2013,** *5* (7), 2302-2315.

17. Jurchescu, O. D.; Popinciuc, M.; van Wees, B. J.; Palstra, T. T. M., Interface-Controlled, High-Mobility Organic Transistors. *Advanced Materials* **2007,** *19* (5), 688-692.

18. Li, H.; Tee, B. C. K.; Cha, J. J.; Cui, Y.; Chung, J. W.; Lee, S. Y.; Bao, Z., High-Mobility Field-Effect Transistors from Large-Area Solution-Grown Aligned C60 Single Crystals. *Journal of the American Chemical Society* **2012,** *134* (5), 2760-2765.

Chapter 1

Comparison of Structural Features and Electron-Donating Strength of Co-Units in Naphthalene Diimide (NDI)-based Copolymers for High-Performance Organic Field-Effect Transistors

I. Introduction

The OFET performance with high mobility in hopping mechanism depends on the molecular structure and packing attributed to low reorganization energy and efficient charge transport.[1] Especially, researches in chemical approach on developing the ideal semiconducting polymers have been focusing on molecular design based on donor–acceptor (D-A) strategy with side-chain engineering considering structure-property relationship for low band gap, energy level, and effective molecular packing.[2] The D-A copolymers consisting of alternating electron deficient and electron rich groups can induce intramolecular charge transfer (ICT) along the polymer backbone.[3]

On the other hand, the high mobility can be achieved from many geometric factors such as coplanar backbone conformation with minimum backbone torsion and steric hindrance between the donor and acceptor units and high degree of in-plane alignment of polymer backbone with edge-on dominant packing and mixed orientation of edge-on and face-on for the 3-D charge transport, as well.[4] The induced lamellar packing with molecularly ordered structure can lead to high crystalline domains with less grain boundaries and defects that interferes the charge transfer between the molecules.[5]

So far, *p*-channel semiconducting polymers with high field-effect mobility and ambient stability have been widely demonstrated with D-A strategy and geometric property analysis.[6] Nowadays some researches have achieved the hole mobility above 10 $cm^2V^{-1}s^{-1}$.[7] Nevertheless, the research on *n*-channel semiconducting polymers requires more challengeable development for high performance and good stability. Highly strong electron-withdrawing group, naphthalene diimide (NDI), has been used as the representative accepting unit for the design of *n*-channel D-A copolymers and generally incorporated with thiophene-based electron-donating groups.[8] After P(NDI2OT-T2)-based thin-film transistors with top-gate bottom-contact configuration was reported as high mobility of 0.85 $cm^2V^{-1}s^{-1}$ in 2009[8f], the different number of thiophene rings and thiophene-based derivatives with various electron donating strength were introduced to produce the high-performance *n*-type semiconducting copolymers.[8]

In this study, NDI-based D-A copolymers with various donating moieties including heteroacene-type (thiophene (Th), selenophene (Se)) and thiophene-free acene-type (benzene (Bz), naphthalene (Np), pyrene (Py)) were studied in energy levels, thin-film morphologies, molecular packing and electrical characteristics in thin-film OFETs. We demonstrated the OFET performance of NDI-based copolymers in the view of structure-property relationship, comparing the geometric factor of the copolymers and electron-donating strength of donor units in the polymer backbone.

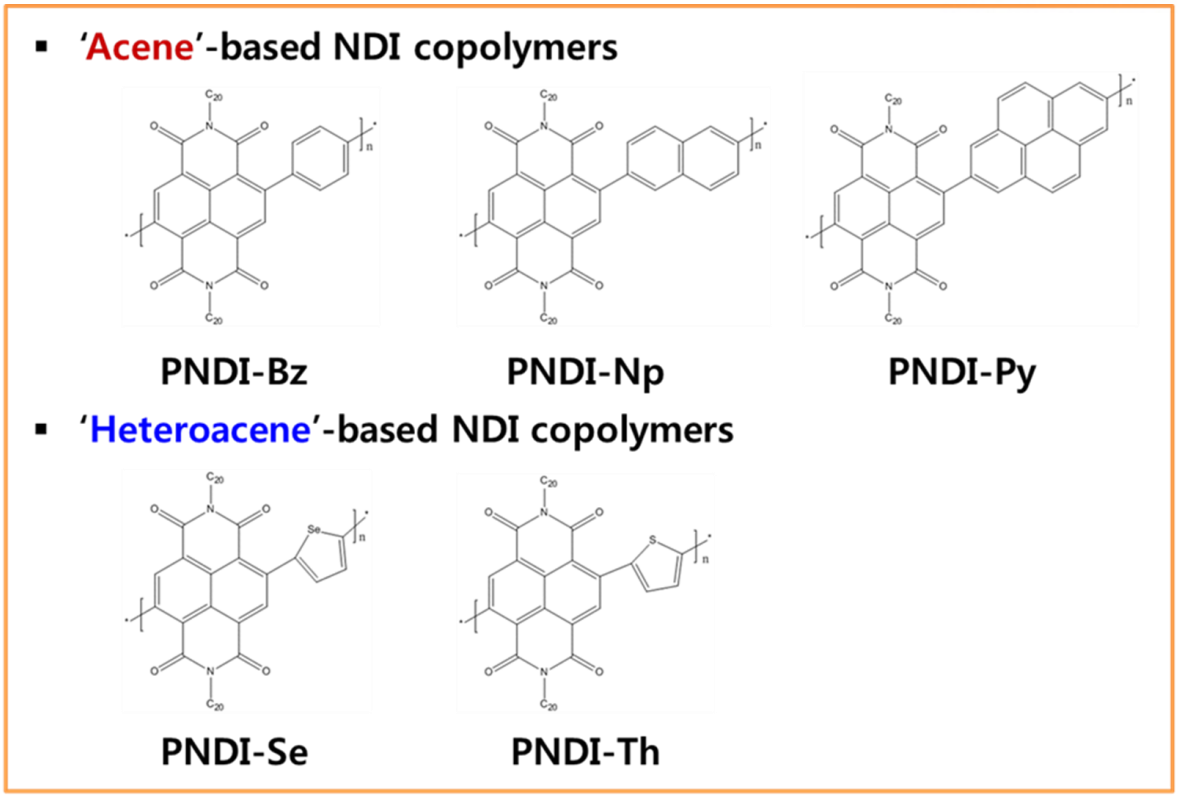

Scheme 1.1. Molecular structures of NDI-based D-A copolymers. (All NDI copolymers were synthesized by Yiho Kim of Prof. Changduk Yang's group, UNIST)

II. Experimental

2.1 Fabrication of NDI-based OFETs

NDI-based OFET devices with bottom-gate top-contact structure were fabricated on the silicon wafer with a heavily n-doped Si and thermally grown 300-nm-thick SiO_2 layer (C_i = 10 nFcm^{-2}). The n-doped Si and SiO_2 layer were utilized as the gate electrode and dielectric, respectively. The surface of SiO_2 layer was modified with self-assembled monolayer, n-octadecyltrimethoxysilane (OTS), in the same method of the previous report.[9] Firstly, we cleaned the SiO_2/Si substrates with piranha solution (a 7:3 mixture of H_2SO_4 and H_2O_2). Then, OTS solution of 3 mM in trichloroethylene was deposited on the SiO_2/Si wafer by spin-coating at 3000 rpm for 30 s. Subsequently, the OTS-coated wafers were placed in a desiccator filled with ammonia vapor. After 12 h, the wafers taken out of the desiccator were washed out with toluene, acetone, and isopropyl alcohol in order. The OTS-treated wafers showed contact angle of ~110° when measured with deionized water. The solution of NDI copolymers dissolved in anhydrous chlorobenzene (~5 mg mL^{-1}) were stirred at 80 ℃ for over 12 h. The film of NDI copolymers was formed by drop-casting the solution on the OTS-treated SiO_2/Si wafer. Drop-cast films were thermally treated on a hot plate at various annealing temperatures (120 ℃, 150 ℃, 180 ℃, and 220 ℃) for 30 min. Source and drain electrodes (Au, 40 nm) were deposited on the film-coated substrate by thermal evaporation through a shadow mask. The channel length (L) and width (W) were 50 μm and 1000 μm, respectively.

2.2 Chracterization of NDI-based OFETs

Thin-film morphology was characterized by X-ray diffractometer (D/MAZX 2500V/PC, Rigaku) in out-of-plane diffraction (2.5° ~ 30°) and tapping-mode atomic force microcope (Agilent 5500, Agilent). The current-voltage characteristics of the devices were measured by Keithley 4200 semiconductor parametric analyzer in a N_2-filled glove box. The field-effect mobility was calculated by the following equation in the saturation regime, $I_{DS} = (1/2)(W/L)\mu C_i(V_G - V_T)^2$, where I_{DS} is the drain current, W and L are the charge transport channel width and length, respectively, μ is the charge carrier mobility, C_i is the capacitance per unit area of the gate dielectric, and V_G and V_T are the gate voltage and threshold voltage, respectively.

III. Results and Discussion

3.1 Characterization of optical and electrochemical properties, and DFT calculation

The molecular structures of NDI-based donor (D)–acceptor (A) copolymers incorporated by various donor groups, benzene (Bz), naphthalene (Np), pyrene (Py), selenophene (Se), and thiophene (Th), are shown in Scheme 1.1. We measured optical and electrochemical properties of all D-A copolymers (PNDI-Bz, PNDI-Np, PNDI-Py, PNDI-Se, and PNDI-Th) to determine the physical features including different conjugation length and conformation/geometry/physical size affected by electron-donating capability of donor moieties.

In the measurement of the absorption spectra of the copolymer films and those of their solutions, we found out that absorption peaks of heteroacene copolymers, PNDI-Se and PNDI-Th, were more red-shifted compared with the acene copolymers, PNDI-Bz, PNDI-Np and PNDI-Py. The intensity of the ICT peaks of PNDI-Se and PNDI-Th was more enhanced relative to the shorter wavelength ones. These results can be explained by stronger donating ability of the heteroacenes units and more efficient ICT formed in heteroacene-based copolymers. (Figure 1.1, Table. 1.1.) Optical bandgaps of NDI-based copolymer was obtained from the absorption edge of the thin film. (2.36 eV for PNDI-Bz, 2.11 eV for PNDI-Np, 1.96 eV for PNDI-Py, 1.79 eV for PNDI-Se, and 1.83 eV for PNDI-Th) The chromatic shifts and bandgaps are determined by electron-donating ability of donor counterpart units in D-A copolymers, giving the donating trend as follows: PNDI-Bz < PNDI-Np < PNDI-Py < PNDI-Th < PNDI-Se, despite the more extended π-conjugation length of Py than other donating units. Interestingly, the vibronic features in the high-energy region (330-410 nm) are more resolved in PNDI-Bz, PNDI-Np, and PNDI-Py than PNDI-Se and PNDI-Th. It suggests that acene-based copolymers have more stiff and well-defined backbones in the solid state.[10]

The LUMO and HOMO energy levels of NDI-based copolymers were investigated by cyclic voltammetry (CV) as shown in Figure 1.2a and Table 1.1. The low-lying LUMO levels can result in n-channel charge transport property in all NDI-based copolymers. We observed the destabilized HOMO levels depending on the electron-donating strength of donor co-units whereas the relatively consistent LUMO levels (-3.73~-3.82 eV) owing to the dominant NDI contribution to the backbone. This result can also support the aforementioned trend of electron-donating ability of donor groups in the sequence of Bz < Np < Py < Th < Se. The relatively high-lying HOMO levels (-5.65~-5.73 eV) in PNDI-Se, PNDI-Th, and PNDI-Py can be considered to enable the hole transport and have ambipolarity in OFETs.

The HOMO/LUMO distributions and geometric structure of the NDI-based copolymers were additionally studied by density functional theory (DFT) computation (B3LYP/6-31G*). (Figure 1.2b) The acene-based copolymers showed the localized HOMO and LUMO electron densities upon the

electron accepting NDI core and the donor counterparts, respectively, while both the HOMOs and LUMOs of the heteroacene-based copolymers are well distributed over the whole backbone. In the view of the geometric structure, the adjacent donor and acceptor units in the molecular backbone of PNDI-Np, PNDI-Se, and PNDI-Th are in the 'eclipsed' position. On the other hand, PNDI-Bz and PNDI-Py showed a 'staggered' shape in moiety planes with 60^{o} torsion angle. PNDI-Py, in particular, exhibited the electron densities concentrated solely on each donor and acceptor unit and the large dihedral angle between NDI and Py units prohibited the effective conjugation system and ICT along the polymer backbone, supporting the reason of relatively wider bandgap. The results of the computational calculation indicated that the interchain π-π stacking, lamellar packing and crystallinity dependent on the charge distributions and curvature in the backbone of the polymers were influenced by the electron-donating properties of donors and the structural features such as conjugation length, geometry, and size.

Table 1.1. Optical and electrochemical properties of NDI-based D-A copolymers.

copolymer	M_n(kDa) /PDI[a]	λ_{max} soln (nm)[b]	λ_{max} film (nm)[c]	E_g^{opt} (eV)[d]	LUMO (eV)[e]	HOMO (eV)[f]
PNDI-Bz	30.8/3.3	457	472	2.36	-3.74	-6.10
PNDI-Np	18.4/2.8	488	514	2.11	-3.78	-5.89
PNDI-Py	3.3/1.4	464	474	1.96	-3.78	-5.73
PNDI-Se	87.8/8.6	574	614	1.79	-3.73	-5.52
PNDI-Th	62.7/5.1	547	600	1.83	-3.82	-5.65

[a]GPC versus polystyrene standards in THF as eluent; [b]Solution absorption spectra in chloroform; [c]Thin film absorption spectra from spin-cast from chloroform solution; [d]Optical energy gap estimated from the absorption onset of the thin films; [e]Cyclic voltammetry determined with Fc/Fc+ as an internal reference (LUMO = -4.8 - ($E_{1/2red}^{first}$- $E_{1/2ox}^{Fe/Fc+}$)); [f]Estimated from HOMO = LUMO – E_g^{opt}.

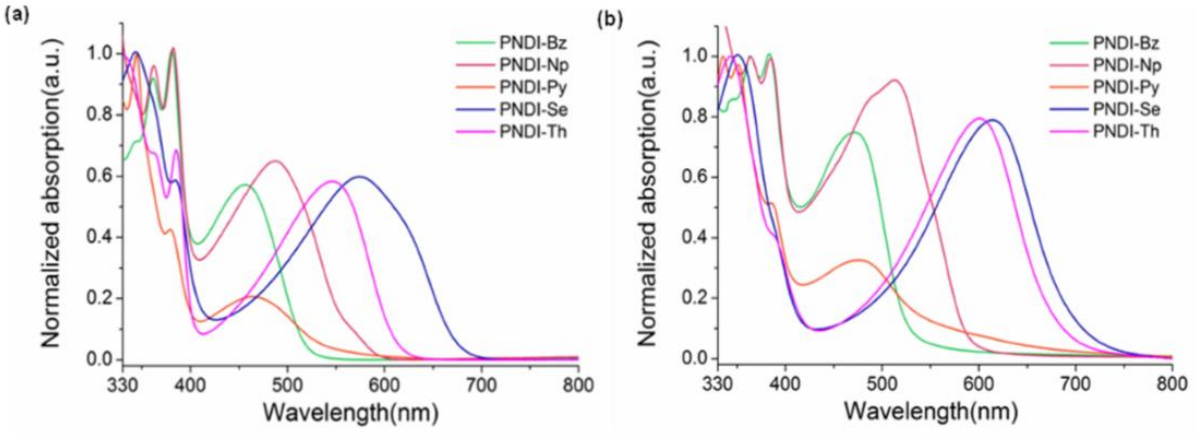

Figure 1.1. Normalized UV-Vis absorption spectra of NDI-based D-A copolymers in (a) chloroform solution and (b) as thin solid films.

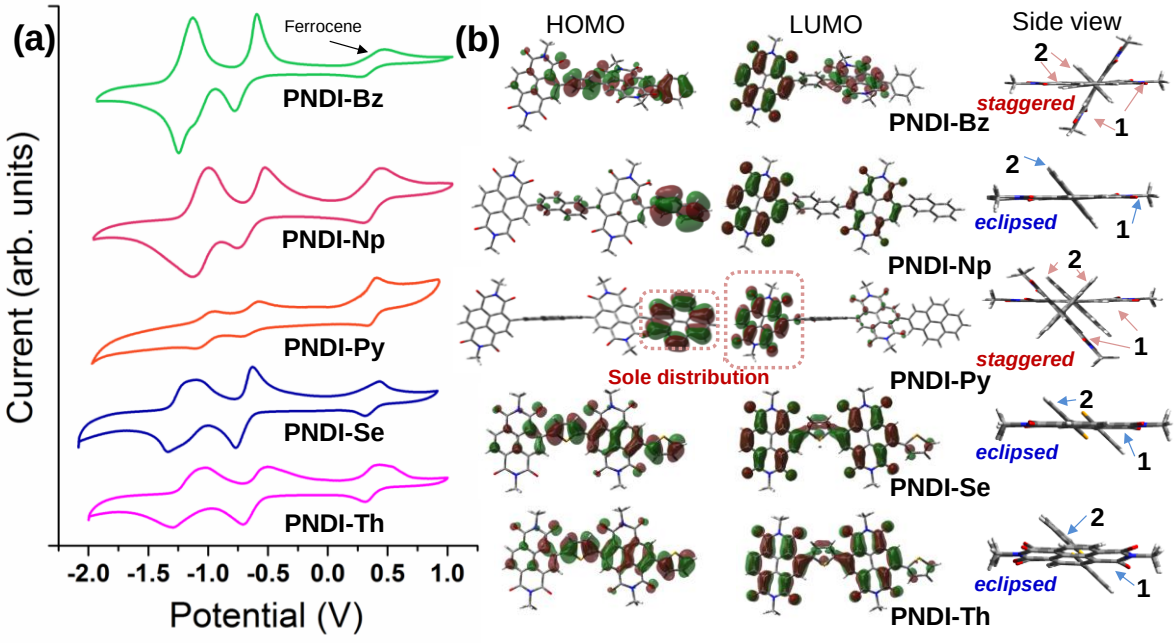

Figure 1.2. (a) Cyclic voltammograms of NDI-based D-A copolymers in thin films drop-cast on a platinum working electrode and tested in n-Bu4NPF6/CH3CN solution (scan rate, 50 mVs-1). (b) Calculated molecular orbitals and optimized geometry for the model dimers of NDI-based copolymers, respectively (B3LYP/6-31G*). (1) and (2) are used to symbolize the NDI acceptor and donor portions, respectively, for clarity of either staggered or eclipsed conformation. The side chains were replaced with methyl groups to simplify the calculation.

3.2 Thin Film Morphology Analyses

The molecular packing of NDI-based copolymers in the thin film were investigated by out-of-plane X-ray diffraction (XRD) analyses, as shown in Figure 1.3 and Table 1.2. Most of the copolymer thin films except for PNDI-Py showed diffraction peak with reduced d(001)-spacing values in the annealed thin films compared with as-cast thin films (Figure S1.1), indicating the denser lamellar packing after annealing. The increased value of d(001)-spacing in PNDI-Py thin films was caused by tend to rotate with regard to the NDI π-planar axis, corresponding to the result of DFT calculations, resulting in less dense molecular packing and interdigitation. From the π-π stacking peaks, we can find out NDI copolymers with less bulky co-units (PNDI-Se, PNDI-Th, and PNDI-Bz) showing broad peaks indicating face-on orientations more easily than those with bulky co-units (PNDI-Np, PNDI-Py). The d-spacing values of π-π stacking peaks in PNDI-Se, PNDI-Th, and PNDI-Bz are relatively larger than other high-performance NDI-based copolymers, inducing less efficient 3-D charge transport.

According to the thin film morphology of NDI-based copolymers measured by tapping-mode atomic-force microscopy (AFM), the annealed films (Figure 1.4) showed formation of relatively larger fibrillar network grains than as-cast films (Figure S1.2), which can result in the higher crystallinity from molecular reorganization for the enhancement of electrical performance.

Table 1.2. Peak assignments for the out-of-plane XRD patterns of as-cast and annealed NDI-based polymer films.

		As-cast Film		Annealed Film[a]	
Polymer	(00n)	2θ (°)	*d(001)*-spacing (Å)	2θ (°)	*d(001)*-spacing (Å)
PNDI-Bz	(001)	3.34	26.43	3.78	23.36
	(002)	-	-	-	-
	(003)	-	-	-	-
	π-stacking	19.68	4.51	19.66	4.51
PNDI-Np	(001)	3.68	23.99	3.70	23.86
	(002)	7.26	-	7.06	-
	(003)	-	-	-	-
	π-stacking	-	-	-	-
PNDI-Py	(001)	3.94	22.41	3.88	22.75
	(002)	7.32	-	7.30	-
	(003)	-	-	-	-
	π-stacking	-	-	-	-
PNDI-Se	(001)	3.73	23.69	4.00	22.08
	(002)	7.38	-	7.22	-
	(003)	12.23	-	12.01	-
	π-stacking	21.32	4.16	21.46	4.14
PNDI-Th	(001)	3.98	22.18	4.18	21.12
	(002)	-	-	-	-
	(003)	-	-	-	-
	π-stacking	21.3	4.17	21.42	4.15

[a]The annealing temperature was chosen as the condition for the best n-channel performance: *i.e.*, **PNDI-Bz** (150 ℃), **PNDI-Np** (150 ℃), **PNDI-Py** (120 ℃), **PNDI-Se** (120 ℃), **PNDI-Th** (150 ℃).

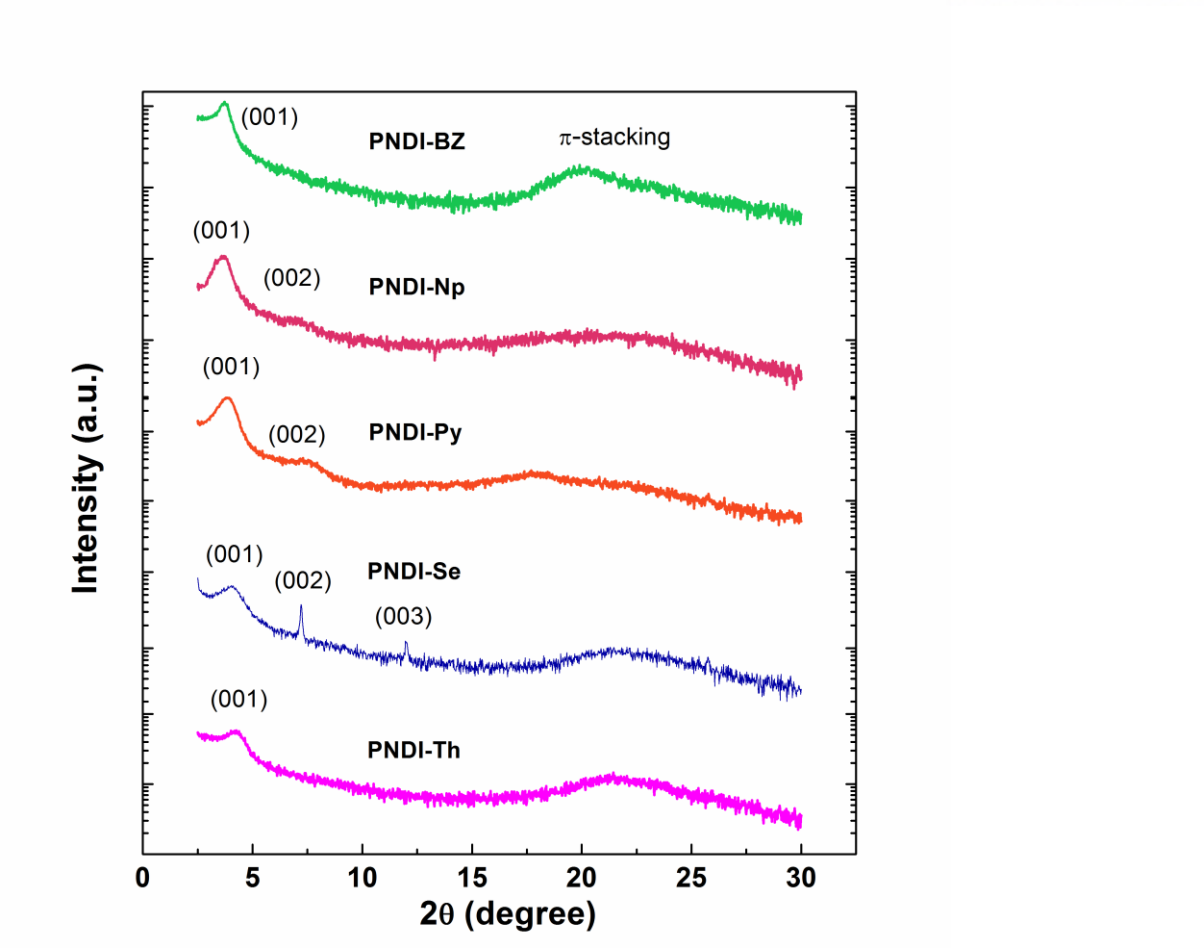

Figure 1.3. Out-of-plane X-ray diffraction (XRD) patterns of the annealed NDI copolymer thin films that show the best n-channel performance.

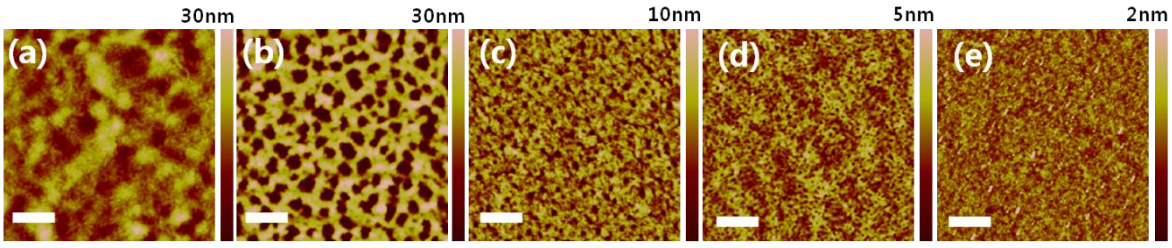

Figure 1.4. AFM height images of (a) **PNDI-Bz**, (b) **PNDI-Np**, (c) **PNDI-Py**, (d) **PNDI-Se**, (e) **PNDI-Th** polymer films annealed at temperatures for the best n-channel performance. Scale bar = 1 μm.

3.3 Electrical Characteristics of NDI-based OFETs

The OFET devices based on NDI copolymers were fabricated in bottom-gate top-contact configuration, as shown in Figure 1.5a. We prepared the OFET devices by solution process with optimized conditions of deposition method and annealing temperature. Compared with the conventional spin-coating method, drop-casting deposition could give the enhanced electrical performance due to the higher crystallinity. The drop-casting method was chosen to prepare thin films, because the wettability of chlorobenzene solution is poor on the highly crystalline OTS-treated SiO_2/Si substrate and the drop-casting method tends to yield a higher crystallinity in the films.

In addition, the thermal treatment was performed at different temperatures, 120, 150, 180, 220 ℃, to achieve the highest mobility at optimized condition. All NDI copolymers showed n-channel characteristics in as-cast films which were considered to be enabled by the low-lying LUMO levels and the electron mobilities were in the range of 10^{-3} ~ 10^{-2} $cm^2V^{-1}s^{-1}$. The electron mobilities of all NDI-based OFETs were clearly enhanced after annealing process at various temperatures, as summarized in Table 1.3 and Figure 1.5b. These results are corresponds to the XRD data and AFM data. The optimized current-voltage (*I-V*) characteristics of NDI-based copolymer OFETs were obtained at 150 ℃ for PNDI-Bz, PNDI-Np, and PNDI-Th, and 120 ℃ for PNDI-Py and PNDI-Se, respectively. The maximum electron mobility was shown in PNDI-Np film with the value of 5.63×10^{-2} $cm^2V^{-1}s^{-1}$, as shown in the typical transfer curves and output characteristics with small degree of hysteresis. (Figure 1.5c). The LUMO windows for NDI copolymers is narrow. Despite the less favorable LUMO level of PNDI-Np for electron injection to the gold contacts, it showed the maximum mobility affected by geometric and morphological features rather than energetic factors. PNDI-Py, PNDI-Th, PNDI-Se that have relatively high-lying HOMO levels making easier hole injection to gold contacts carriers compared with PNDI-Bz and PNDI-Np showing only unipolar n-channel characteristics showed ambipolar charge transport after thermal annealing at a high temperature. (Figure S1.2) Also the well-delocalized HOMOs and LUMOs of PNDI-Se and PNDI-Th can support the ambipolar characteristics. The PNDI-Py have extended π-conjugation length in basic unit but effective conjugation system and ICT along the main backbone were prohibited due to the large dihedral angle between NDI and Py units from DFT calculation resulting in solely concentrated electron densities in HOMO and LUMO and wider bandgap than heteroacene-based copolymers, PNDI-Se and PNDI-Th. Although the annealed films of PNDI-Py showed increased d(001)-spacing value in XRD data because of slightly tilted pyrene moiety, they also showed higher mobility than as-cast film due to larger co-facing stack area of π-planes.

Table 1.3. *I-V* characteristics of NDI-based copolymer OFETs obtained at different annealing temperatures.

		n-channel				*p*-channel			
Polymer	T_a [°C]	I_{on}/I_{off}	V_{th} [V]	$\mu_{e,avg}$[b] [$cm^2/V \cdot s$]	$\mu_{e,max}$[c] [$cm^2/V \cdot s$]	I_{on}/I_{off}	V_{th} [V]	$\mu_{h,avg}$[b] [$cm^2/V \cdot s$]	$\mu_{h,max}$[c] [$cm^2/V \cdot s$]
PNDI-Bz	N/A[a]	9.7×10^3	22.6	2.8×10^{-3}	4.9×10^{-3}	-[d]	-	-	-
	120	1.3×10^5	44.3	3.3×10^{-3}	5.3×10^{-3}	-	-	-	-
	150	1.1×10^4	37.0	5.5×10^{-3}	8.0×10^{-3}	-	-	-	-
	180	1.3×10^5	30.4	4.1×10^{-3}	5.7×10^{-3}	-	-	-	-
	220	3.0×10^5	26.4	2.1×10^{-3}	2.6×10^{-3}	-	-	-	-
PNDI-Np	N/A	3.0×10^5	30.0	1.0×10^{-2}	1.6×10^{-2}	-	-	-	-
	120	8.3×10^4	28.2	2.1×10^{-2}	2.6×10^{-2}	-	-	-	-
	150	2.7×10^5	30.6	4.0×10^{-2}	5.6×10^{-2}	-	-	-	-
	180	3.0×10^3	27.9	3.6×10^{-2}	5.6×10^{-2}	-	-	-	-
	220	2.1×10^5	27.3	1.6×10^{-2}	2.2×10^{-2}	-	-	-	-
PNDI-Py	N/A	3.9×10^4	24.5	1.2×10^{-3}	2.7×10^{-3}	-	-	-	-
	120	4.7×10^4	31.4	4.5×10^{-3}	7.6×10^{-3}	1.1×10^2	-109.5	8.7×10^{-5}	7.4×10^{-4}
	150	5.2×10^5	36.2	3.6×10^{-3}	7.5×10^{-3}	6.7×10^1	-120.8	1.5×10^{-4}	9.3×10^{-4}
	180	2.0×10^6	13.9	2.6×10^{-3}	4.9×10^{-3}	6.2×10^1	-89.7	5.0×10^{-5}	4.0×10^{-4}
	220	4.6×10^5	17.7	2.2×10^{-3}	4.8×10^{-3}	5.3×10^1	-82.8	7.5×10^{-5}	3.6×10^{-4}
PNDI-Se	N/A	3.5×10^4	28.1	6.0×10^{-3}	7.9×10^{-3}	-	-	-	-
	120	5.9×10^4	32.7	1.5×10^{-2}	2.2×10^{-2}	-	-	-	-
	150	1.8×10^5	31.3	9.1×10^{-3}	1.7×10^{-2}	-	-	-	-
	180	9.6×10^4	14.3	7.5×10^{-3}	1.0×10^{-2}	-	-	-	-
	220	3.0×10^5	21.4	8.2×10^{-3}	1.3×10^{-2}	1.2×10^1	-140.6	6.5×10^{-6}	2.2×10^{-5}
PNDI-Th	N/A	1.5×10^5	14.0	3.8×10^{-3}	7.6×10^{-3}	-	-	-	-
	120	5.5×10^4	29.2	6.1×10^{-3}	8.7×10^{-3}	-	-	-	-
	150	6.7×10^5	17.0	1.1×10^{-2}	1.9×10^{-2}	-	-	-	-
	180	6.2×10^5	-2.9	1.0×10^{-2}	1.7×10^{-2}	-	-	-	-
	220	3.1×10^5	-9.2	1.1×10^{-2}	3.2×10^{-2}	7.8×10^2	-113.6	1.2×10^{-4}	6.9×10^{-4}

[a]The thermal annealing was not applied. [b]The average and [c]the maximum mobility of the OFET devices (L = 50 μm and W = 1000 μm). [d]The p-channel behavior was not observed.

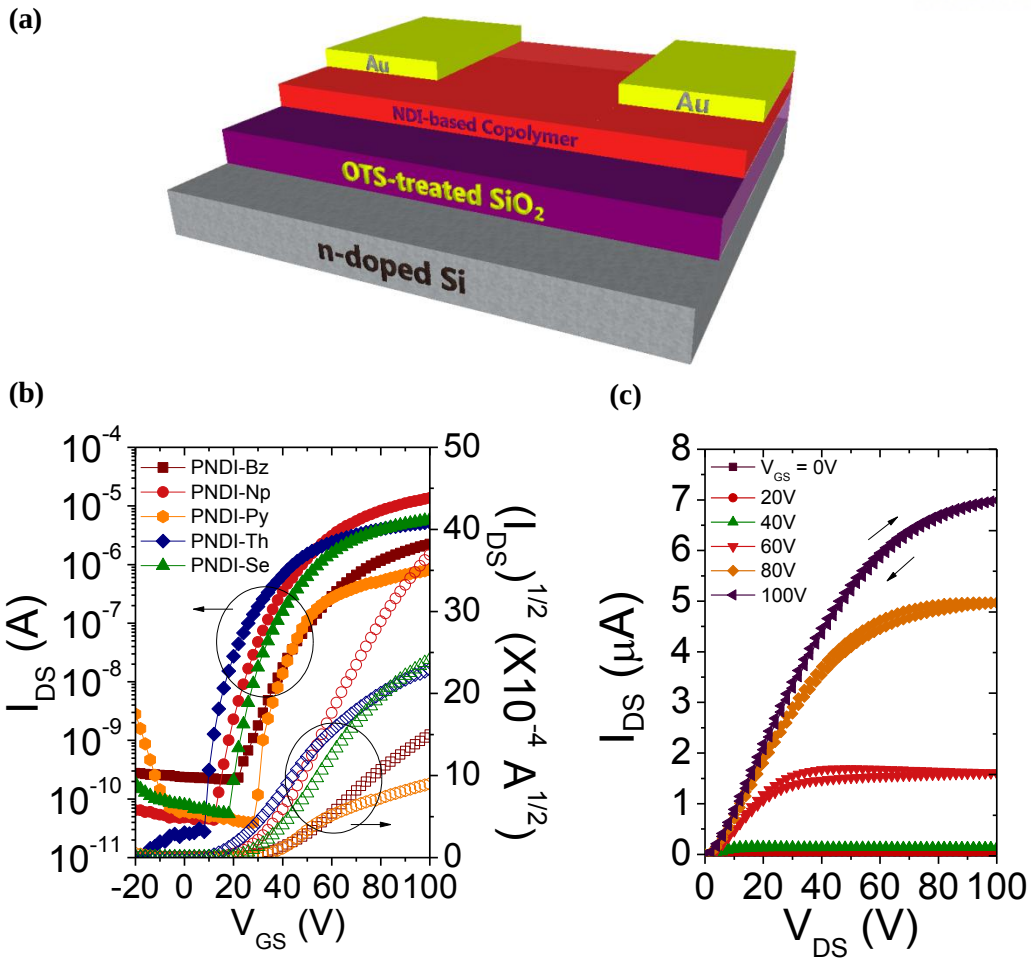

Figure 1.5. (a) Schematic illustration of OFET in BGTC structure. (b) Optimized n-channel transfer characteristics of OFETs based on annealed NDI copolymer thin films. (c) Output characteristics of the best-performing n-channel **PNDI-Np** OFET annealed at 150 ℃.

IV. Conclusion

We demonstrated the structure-property relationship for the OFETs based on NDI-based D-A copolymers (‘acene’-based PNDI-Bz, PNDI-Np, and PNDI-Py, ‘heteroacene’-based PNDI-Th, and PNDI-Se) comparing the influence of geometric features with electron-donating strength of donor units in the polymer backbone. From the results of optical and electrochemical properties, NDI-based copolymers exhibited the donor strengths in the increasing order of Bz, Np, Py, Th, and Se, allowing more efficient ICT in the backbone of the copolymers. All the polymers showed n-channel dominant transport in thin-film transistors deposited by drop-casting and annealed at various temperatures. According to the HOMO levels positioned by electron-donating ability of donor counterparts, the copolymers, PNDI-Bz and PNDI-Np, showed unipolar n-channel characteristics while PNDI-Py, PNDI-Se, and PNDI-Th with high-lying HOMO levels showed ambipolar characteristics. Regardless of the donating capability of donor groups, the highest electron mobility was obtained in acene-based PNDI-Np (5.63×10^{-2} $cm^2V^{-1}s^{-1}$) which has centrosymmetric structure with ‘eclipsed’ shape in backbone moiety planes among the other copolymers. This result can suggest the importance of molecular packing and intermolecular interaction by physical structure as well as the electron-donating strength of donors in the NDI-based D-A copolymers for high-performance organic transistor device.

V. Reference

1. Sirringhaus, H., 25th Anniversary Article: Organic Field-Effect Transistors: The Path Beyond Amorphous Silicon. *Advanced Materials* **2014,** *26* (9), 1319-1335.

2. Dong, H.; Fu, X.; Liu, J.; Wang, Z.; Hu, W., 25th Anniversary Article: Key Points for High-Mobility Organic Field-Effect Transistors. *Advanced Materials* **2013,** *25* (43), 6158-6183.

3. (a) Cho, S.; Lee, J.; Tong, M.; Seo, J. H.; Yang, C., Poly(diketopyrrolopyrrole-benzothiadiazole) with Ambipolarity Approaching 100% Equivalency. *Adv. Funct. Mater.* **2011,** *21* (10), 1910-1916; (b) Dutta, G. K.; Han, A. R.; Lee, J.; Kim, Y.; Oh, J. H.; Yang, C., Visible-Near Infrared Absorbing Polymers Containing Thienoisoindigo and Electron-Rich Units for Organic Transistors with Tunable Polarity. *Adv. Funct. Mater.* **2013**, n/a-n/a; (c) Lee, J.; Han, A. R.; Hong, J.; Seo, J. H.; Oh, J. H.; Yang, C., Inversion of Dominant Polarity in Ambipolar Polydiketopyrrolopyrrole with Thermally Removable Groups. *Adv. Funct. Mater.* **2012,** *22* (19), 4128-4138; (d) Osaka, I.; Sauvé, G.; Zhang, R.; Kowalewski, T.; McCullough, R. D., Novel Thiophene-Thiazolothiazole Copolymers for Organic Field-Effect Transistors. *Adv. Mater.* **2007,** *19* (23), 4160-4165; (e) Ando, S.; Nishida, J.-i.; Tada, H.; Inoue, Y.; Tokito, S.; Yamashita, Y., High Performance n-Type Organic Field-Effect Transistors Based on π-Electronic Systems with Trifluoromethylphenyl Groups. *J. Am. Chem. Soc.* **2005,** *127* (15), 5336-5337; (f) Jenekhe, S. A.; Lu, L.; Alam, M. M., New Conjugated Polymers with Donor−Acceptor Architectures: Synthesis and Photophysics of Carbazole−Quinoline and Phenothiazine−Quinoline Copolymers and Oligomers Exhibiting Large Intramolecular Charge Transfer. *Macromolecules* **2001,** *34* (21), 7315-7324; (g) Zhou, H.; Yang, L.; You, W., Rational Design of High Performance Conjugated Polymers for Organic Solar Cells. *Macromolecules* **2012,** *45* (2), 607-632.

4. (a) Sirringhaus, H.; Brown, P. J.; Friend, R. H.; Nielsen, M. M.; Bechgaard, K.; Langeveld-Voss, B. M. W.; Spiering, A. J. H.; Janssen, R. A. J.; Meijer, E. W.; Herwig, P.; de Leeuw, D. M., Two-dimensional charge transport in self-organized, high-mobility conjugated polymers. *Nature* **1999,** *401* (6754), 685-688; (b) Li, J.; Zhao, Y.; Tan, H. S.; Guo, Y.; Di, C.-A.; Yu, G.; Liu, Y.; Lin, M.; Lim, S. H.; Zhou, Y.; Su, H.; Ong, B. S., A stable solution-processed polymer semiconductor with record high-mobility for printed transistors. *Sci. Rep.* **2012,** *2*; (c) Rivnay, J.; Steyrleuthner, R.; Jimison, L. H.; Casadei, A.; Chen, Z.; Toney, M. F.; Facchetti, A.; Neher, D.; Salleo, A., Drastic Control of Texture in a High Performance n-Type Polymeric Semiconductor and Implications for Charge Transport. *Macromolecules* **2011,** *44* (13), 5246-5255.

5. (a) Lei, T.; Cao, Y.; Zhou, X.; Peng, Y.; Bian, J.; Pei, J., Systematic Investigation of Isoindigo-Based Polymeric Field-Effect Transistors: Design Strategy and Impact of Polymer Symmetry and Backbone Curvature. *Chemistry of Materials* **2012,** *24* (10), 1762-1770; (b) Brock, C. P.; Dunitz, J. D., Temperature dependence of thermal motion in crystalline anthracene. *Acta Crystallographica Section B* **1990,** *46* (6), 795-806; (c) Coropceanu, V.; Cornil, J.; da Silva Filho, D. A.; Olivier, Y.; Silbey, R.; Brédas, J.-L., Charge Transport in Organic Semiconductors. *Chemical Reviews* **2007,** *107* (4), 926-952.

6. (a) Park, J. H.; Jung, E. H.; Jung, J. W.; Jo, W. H., A Fluorinated Phenylene Unit as a Building Block for High-Performance n-Type Semiconducting Polymer. *Adv. Mater.* **2013,** *25* (18), 2583-2588; (b) Kang, I.; An, T. K.; Hong, J.-A.; Yun, H.-J.; Kim, R.; Chung, D. S.; Park, C. E.; Kim, Y.-H.; Kwon, S.-K., Effect of Selenophene in a DPP Copolymer Incorporating a Vinyl Group for High-Performance Organic Field-Effect Transistors. *Adv. Mater.* **2013,** *25* (4), 524-528; (c) Usta, H.; Newman, C.; Chen, Z.; Facchetti, A., Dithienocoronenediimide-Based Copolymers as Novel Ambipolar Semiconductors for Organic Thin-Film Transistors. *Adv. Mater.* **2012,** *24* (27), 3678-3684; (d) Lei, T.; Dou, J.-H.; Pei, J., Influence of Alkyl Chain Branching Positions on the Hole Mobilities of Polymer Thin-Film

Transistors. *Adv. Mater.* **2012,** *24* (48), 6457-6461; (e) Lei, T.; Dou, J.-H.; Ma, Z.-J.; Yao, C.-H.; Liu, C.-J.; Wang, J.-Y.; Pei, J., Ambipolar Polymer Field-Effect Transistors Based on Fluorinated Isoindigo: High Performance and Improved Ambient Stability. *J. Am. Chem. Soc.* **2012,** *134* (49), 20025-20028; (f) Lee, J. S.; Son, S. K.; Song, S.; Kim, H.; Lee, D. R.; Kim, K.; Ko, M. J.; Choi, D. H.; Kim, B.; Cho, J. H., Importance of Solubilizing Group and Backbone Planarity in Low Band Gap Polymers for High Performance Ambipolar field-effect Transistors. *Chem. Mater.* **2012,** *24* (7), 1316-1323; (g) Kronemeijer, A. J.; Gili, E.; Shahid, M.; Rivnay, J.; Salleo, A.; Heeney, M.; Sirringhaus, H., A Selenophene-Based Low-Bandgap Donor–Acceptor Polymer Leading to Fast Ambipolar Logic. *Adv. Mater.* **2012,** *24* (12), 1558-1565; (h) Kanimozhi, C.; Yaacobi-Gross, N.; Chou, K. W.; Amassian, A.; Anthopoulos, T. D.; Patil, S., Diketopyrrolopyrrole–Diketopyrrolopyrrole-Based Conjugated Copolymer for High-Mobility Organic Field-Effect Transistors. *J. Am. Chem. Soc.* **2012,** *134* (40), 16532-16535; (i) Chen, Z.; Lee, M. J.; Shahid Ashraf, R.; Gu, Y.; Albert-Seifried, S.; Meedom Nielsen, M.; Schroeder, B.; Anthopoulos, T. D.; Heeney, M.; McCulloch, I.; Sirringhaus, H., High-Performance Ambipolar Diketopyrrolopyrrole-Thieno[3,2-b]thiophene Copolymer Field-Effect Transistors with Balanced Hole and Electron Mobilities. *Adv. Mater.* **2012,** *24* (5), 647-652; (j) Chen, H.; Guo, Y.; Yu, G.; Zhao, Y.; Zhang, J.; Gao, D.; Liu, H.; Liu, Y., Highly π-Extended Copolymers with Diketopyrrolopyrrole Moieties for High-Performance Field-Effect Transistors. *Adv. Mater.* **2012,** *24* (34), 4618-4622; (k) Tsao, H. N.; Cho, D. M.; Park, I.; Hansen, M. R.; Mavrinskiy, A.; Yoon, D. Y.; Graf, R.; Pisula, W.; Spiess, H. W.; Müllen, K., Ultrahigh Mobility in Polymer Field-Effect Transistors by Design. *J. Am. Chem. Soc.* **2011,** *133* (8), 2605-2612; (l) Mohebbi, A. R.; Yuen, J.; Fan, J.; Munoz, C.; Wang, M. f.; Shirazi, R. S.; Seifter, J.; Wudl, F., Emeraldicene as an Acceptor Moiety: Balanced-Mobility, Ambipolar, Organic Thin-Film Transistors. *Adv. Mater.* **2011,** *23* (40), 4644-4648; (m) Mei, J.; Kim, D. H.; Ayzner, A. L.; Toney, M. F.; Bao, Z., Siloxane-Terminated Solubilizing Side Chains: Bringing Conjugated Polymer Backbones Closer and Boosting Hole Mobilities in Thin-Film Transistors. *J. Am. Chem. Soc.* **2011,** *133* (50), 20130-20133; (n) Li, Y.; Sonar, P.; Singh, S. P.; Soh, M. S.; van Meurs, M.; Tan, J., Annealing-Free High-Mobility Diketopyrrolopyrrole−Quaterthiophene Copolymer for Solution-Processed Organic Thin Film Transistors. *J. Am. Chem. Soc.* **2011,** *133* (7), 2198-2204; (o) Lei, T.; Cao, Y.; Fan, Y.; Liu, C.-J.; Yuan, S.-C.; Pei, J., High-Performance Air-Stable Organic Field-Effect Transistors: Isoindigo-Based Conjugated Polymers. *J. Am. Chem. Soc.* **2011,** *133* (16), 6099-6101; (p) Ha, J. S.; Kim, K. H.; Choi, D. H., 2,5-Bis(2-octyldodecyl)pyrrolo[3,4-c]pyrrole-1,4-(2H,5H)-dione-Based Donor−Acceptor Alternating Copolymer Bearing 5,5′-Di(thiophen-2-yl)-2,2′-biselenophene Exhibiting 1.5 cm2·V−1·s−1 Hole Mobility in Thin-Film Transistors. *J. Am. Chem. Soc.* **2011,** *133* (27), 10364-10367; (q) Bronstein, H.; Chen, Z.; Ashraf, R. S.; Zhang, W.; Du, J.; Durrant, J. R.; Shakya Tuladhar, P.; Song, K.; Watkins, S. E.; Geerts, Y.; Wienk, M. M.; Janssen, R. A. J.; Anthopoulos, T.; Sirringhaus, H.; Heeney, M.; McCulloch, I., Thieno[3,2-b]thiophene−Diketopyrrolopyrrole-Containing Polymers for High-Performance Organic Field-Effect Transistors and Organic Photovoltaic Devices. *J. Am. Chem. Soc.* **2011,** *133* (10), 3272-3275; (r) Zhang, W.; Smith, J.; Watkins, S. E.; Gysel, R.; McGehee, M.; Salleo, A.; Kirkpatrick, J.; Ashraf, S.; Anthopoulos, T.; Heeney, M.; McCulloch, I., Indacenodithiophene Semiconducting Polymers for High-Performance, Air-Stable Transistors. *J. Am. Chem. Soc.* **2010,** *132* (33), 11437-11439; (s) Li, Y.; Singh, S. P.; Sonar, P., A High Mobility P-Type DPP-Thieno[3,2-b]thiophene Copolymer for Organic Thin-Film Transistors. *Adv. Mater.* **2010,** *22* (43), 4862-4866.

7. (a) Li, J.; Zhao, Y.; Tan, H. S.; Guo, Y.; Di, C.-A.; Yu, G.; Liu, Y.; Lin, M.; Lim, S. H.; Zhou, Y.; Su, H.; Ong, B. S., A stable solution-processed polymer semiconductor with record high-mobility for printed transistors. *Sci. Rep.* **2012,** *2*, 754; (b) Kang, I.; Yun, H.-J.; Chung, D. S.; Kwon, S.-K.; Kim, Y.-H., Record High Hole Mobility in Polymer Semiconductors via Side-Chain Engineering. *Journal of the*

American Chemical Society **2013,** *135* (40), 14896-14899.

8. (a) Guo, X.; Kim, F. S.; Seger, M. J.; Jenekhe, S. A.; Watson, M. D., Naphthalene Diimide-Based Polymer Semiconductors: Synthesis, Structure–Property Correlations, and n-Channel and Ambipolar Field-Effect Transistors. *Chemistry of Materials* **2012,** *24* (8), 1434-1442; (b) Hwang, Y.-J.; Ren, G.; Murari, N. M.; Jenekhe, S. A., n-Type Naphthalene Diimide–Biselenophene Copolymer for All-Polymer Bulk Heterojunction Solar Cells. *Macromolecules* **2012,** *45* (22), 9056-9062; (c) Durban, M. M.; Kazarinoff, P. D.; Luscombe, C. K., Synthesis and Characterization of Thiophene-Containing Naphthalene Diimide n-Type Copolymers for OFET Applications. *Macromolecules* **2010,** *43* (15), 6348-6352; (d) Hwang, Y.-J.; Murari, N. M.; Jenekhe, S. A., New n-type polymer semiconductors based on naphthalene diimide and selenophene derivatives for organic field-effect transistors. *Polymer Chemistry* **2013,** *4* (11), 3187-3195; (e) Wurthner, F.; Stolte, M., Naphthalene and perylene diimides for organic transistors. *Chemical Communications* **2011,** *47* (18), 5109-5115; (f) Yan, H.; Chen, Z.; Zheng, Y.; Newman, C.; Quinn, J. R.; Dötz, F.; Kastler, M.; Facchetti, A., A high-mobility electron-transporting polymer for printed transistors. *Nature* **2009,** *457* (7230), 679-686.

9. Ito, Y.; Virkar, A. A.; Mannsfeld, S.; Oh, J. H.; Toney, M.; Locklin, J.; Bao, Z., Crystalline Ultrasmooth Self-Assembled Monolayers of Alkylsilanes for Organic Field-Effect Transistors. *J. Am. Chem. Soc.* **2009,** *131* (26), 9396-9404.

10. (a) Braun, D.; Heeger, A. J., Visible light emission from semiconducting polymer diodes. *Appl. Phys. Lett.* **1991,** *58* (18), 1982-1984; (b) Balan, B.; Vijayakumar, C.; Saeki, A.; Koizumi, Y.; Tsuji, M.; Seki, S., Optical and electrical properties of dithienothiophene based conjugated polymers: medium donor vs. weak, medium, and strong acceptors. *Polym. Chem.* **2013,** *4* (7), 2293-2303.

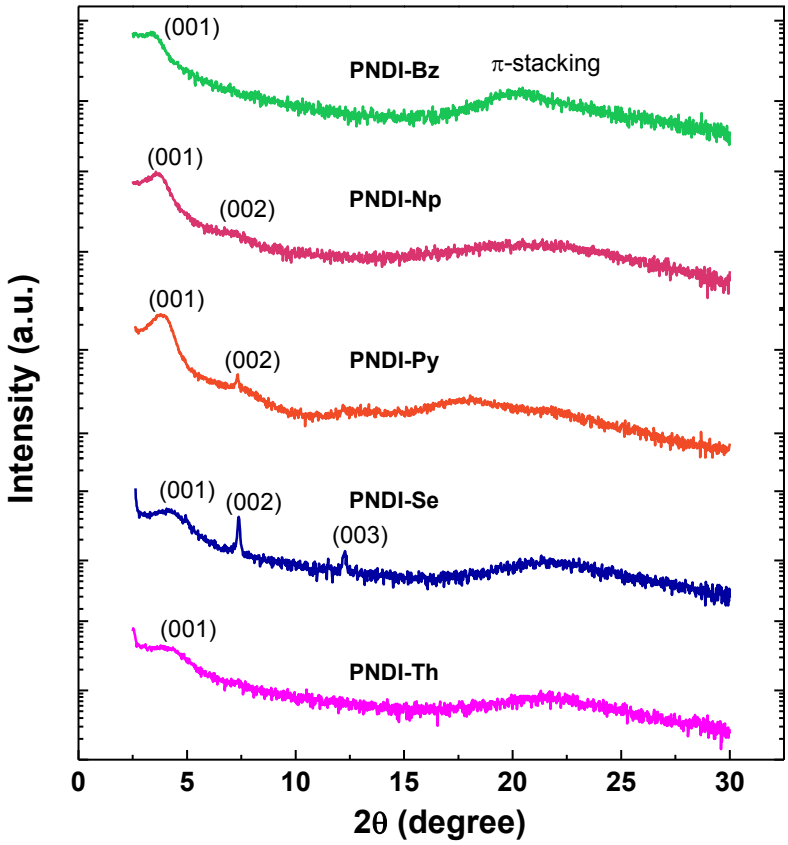

Figure S1.1. Out-of-plane X-ray diffraction (XRD) patterns of the as-cast NDI copolymer thin films.

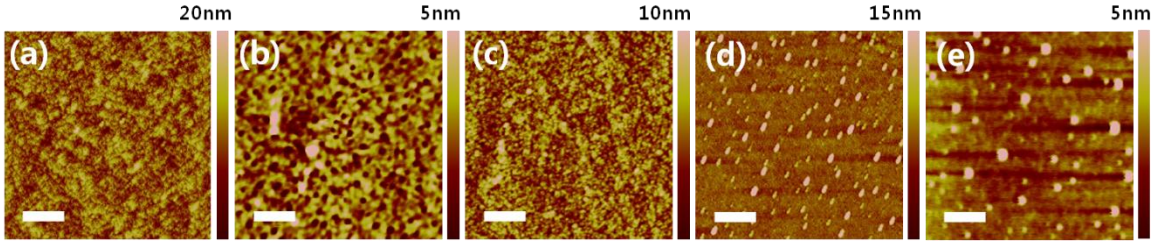

Figure S1.2. AFM height images of (a) **PNDI-Bz**, (b) **PNDI-Np**, (c) **PNDI-Py**, (d) **PNDI-Se**, (e) **PNDI-Th** as-cast films. Scale bar = 1 μm.

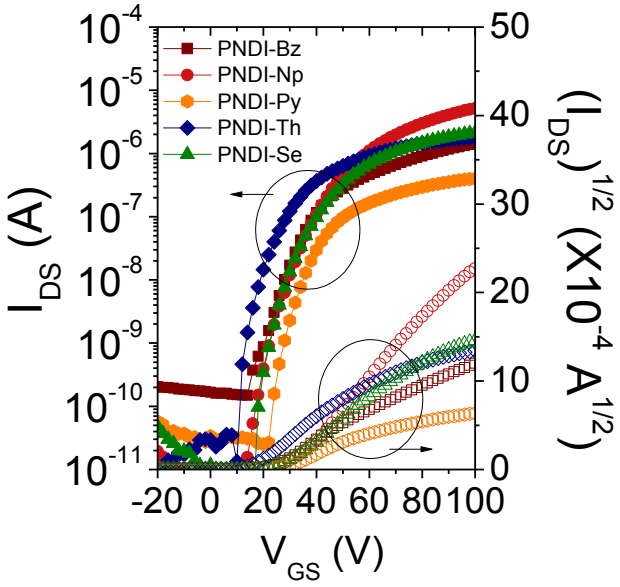

Figure S1.3. Transfer curves of OFETs based on the as-cast NDI copolymer films.

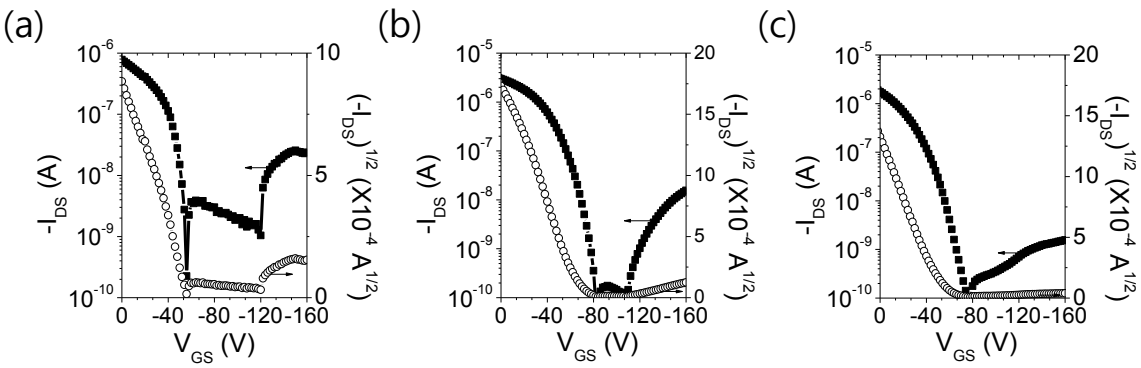

Figure S1.4. Transfer characteristics of (a) **PNDI-Py** annealed at 120 ℃, (b) **PNDI-Th** and (b) **PNDI-Se** annealed at 220 ℃ at hole-enhancement operation.

Chapter 2

Textile-Based Organic Field-Effect Transistors and Application to Wearable Photosensors with High Flexibility and Mechanical Stability

I. Introduction

Wearable electronic devices have attracted great interest for their potential use in healthcare monitoring system, military instruments, public safety, and portable electronic devices. OFET-based sensors are the prospective representatives for the application to wearable sensor devices due to the advantages of OFETs such as low cost, light weight, and flexibility as mentioned at the beginning.[1]

To develop the highly flexible OFETs, a number of researches were reported with regard to the components in the device such as flexible substrates, polymeric dielectric materials, and nanostructured organic semiconducting materials.[2] In particular, various kinds of substrates such as polymer films, textile, elastomeric polymers, yarns, and papers were demonstrated for achieving the stable electrical characteristics.[3] Among the various substrates, textile has been considered to be one of the strong candidates for the novel substrate with high flexibility, and even stretchability that can be used directly in the clothing or objects with fabric.[3e, 3j, 4]

In addition, for the application of OFET-based sensors, organic semiconducting nanomaterials are preferred to be used as active layer rather than thin films because they have features of high electrical property, high-aspect-ratio for high sensitivity, good applicability to flexible devices, and photo-responsivity induced from their prominent crystallinity.[5] Therefore, they have been promising constituent for the active channel in OFETs and OFET-based sensors, especially photosensors.

In this work, highly flexible textile-based image sensors have been demonstrated with electrospun photo-responsive semiconducting nanofiber based on poly(3,3‴-didodecylquaterthiophene) (PQT-12). High flexibility has been accomplished by introduction of textile substrate and polymer dielectrics as polyethylene terephthalate (PET) textile and poly(dimethylsiloxane) (PDMS), respectively. The textile-based OFETs showed negligible degradation of the electrical performance down to extremely small bending radius (up to 0.75 mm) and cycles of bending test (up to 1,000 cycles), confirming high mechanical stability of the textile-based devices. Moreover, photo sensing test has been demonstrated with electrospun PQT-12 nanofibers. Analysis of drain current responses toward different wavelengths of light have successfully been conducted the results were well matched with absorption spectra of the semiconductor. Finally, two-dimensional image sensing also has been processed with 10×10 array of textile-based OFETs, providing possibility of the devices to utilize them as wearable photo sensors.

II. Experimental

2.1 Preparation of textile-based OFET substrate

We used commercially available plain woven PET textile as substrate of the OFET device with bottom-gate bottom-contact (BGBC) configuration. The diameter of the fiber in the PET textile was 40 μm. The shortest distance between the adjacent fibers was 60 μm. For the fabrication of the device, PET textile was washed with acetone, blown by nitrogen gas stream, and dried at room temperature. In order to form the buffered flat surface on the textile by filling up the open spaces, the mixture of PDMS monomer and cross-linker (10:1, weight ratio) were poured over the textile on the slide glass and sandwiched by the other slide glass. After curing PDMS at 80 ℃ for 6 h and removing the slide glass, the thickness of PDMS-buffered PET textile was about 100 μm. Then, chrome (Cr) and gold (Au) were thermally evaporated in sequence through the shadow mask on the textile substrate to be utilized as the gate electrode. The thickness of chrome and gold was 5 nm and 100 nm, respectively. The PDMS dielectric layer was prepared by spin-coating the blend of PDMS monomer, cross-linker, and trichloroethylene (10:1:30, weight ratio) on the OTS-treated SiO_2 substrate. After curing process at 150 ℃ for 1 h, the PDMS dielectric layer was transferred to the gate-patterned textile substrate. The patterned source/drain gold electrodes with thickness of 40 nm were deposited through shadow mask by thermal evaporation.

2.2 Fabrication of PQT-12:PEO nanofibers

As the active channel of the OFET device, PQT-12-based nanofibers were directly deposited on the textile-based substrate by electrospinning. (Figure 2.1) The mixture solution of PQT-12 (M_w 50,000~150,000, Solaris. Chem.) and poly(ethylene oxide) (PEO) (M_w ~600,000, Sigma Aldrich) in chlorobenzene were prepared with total concentration of 10 wt% in 2:1 weight ratio. (Scheme 2.1) To dissolve the solutes completely, the solution was heated and stirred on the hot plate at 60 ℃ for about 24 h. Electrospinning PQT-12:PEO nanofibers was conducted at 15 kV through a single nozzle (inner diameter = 0.33 mm) with the feeding rate of 10 μL min^{-1}. The nozzle-to-collector distance was 10 cm. Electrospun PQT-12:PEO nanofibers were collected to the substrates attached on drum collector rotating with speed of 1500 rpm for the alignment of nanofibers to form the charge transport channel between source and drain electrode.

2.3 Characterization of textile-based OFET devices

Textile-based OFET device and electrospun nanofibers were observed by optical microscopy (OM, Olympus BX53) and field-emission scanning electron microscopy (FE-SEM, Hitachi S-4800). The electrical performance of textile-based OFETs was characterized by Keithley 4200-SCS semiconductor parametric analyzer. (V_{GS} = 60 to -100 V, V_{DS} = -100 V) Electrical performance of PQT-12:PEO nanofibers on conventional Si wafer was measured on highly n-doped Si substrate with OTS-treated SiO_2(300 nm) layer and Cr/Au electrode (4/40 nm). (V_{GS} = 60 to -100 V, V_{DS} = -100 V) The coplanar-gate transistors fabricated on polyimide (PI) substrate with patterned gate and source/drain electrodes (Au/Cr, 40 nm/4 nm) contained electrospun PQT-12:PEO nanofibers and ion-gel dielectric (a mixture of the 1-ethyl-3-methylimidazolium bis(trifluoromethyl sulfonyl)imide ([EMIM][TFSI]) ion liquid, poly(ethylene glycol) diacrylate (PEGDA) monomer, and 2-hydroxy-2methylpropiophenone (HOMPP) photo-initiator (weight ratio of 88:8:4), drop-cast and crosslinked by UV light (365 nm, 25 $mWcm^{-2}$, 8 s)). Coplanar-gate-structured OFET devices were measured under V_{GS} = 1 to -3 V and V_{DS} = -1 V.

The bending test on the cylindrical objects with various bending radius (6.7, 4.6, 3.5, 2.7, 1.6, and 0.75 mm) was performed. The electrical characteristics under the bending cycle test at bending radius of 2.5 mm was measured every 100 cycles during 1000 cycles. Optical property of pure PQT-12 and PQT-12:PEO in solution and thin-film, and PQT-12:PEO nanofiber was measured by uv-visible spectroscopy (JASCO V-670 spectrophotometer). The characterization of optoelectronic properties of textile-based OFET device was conducted under monochromatic laser source (Oriel Cornerstone^{TM} 130 1/8 m Monochromator) and polychromatic source of optical microscope (FOK-160W, Fiber Optic Korea). The intensities of light source were 100 μW cm^{-2} for monochromatic light, and 6 mW cm^{-2} for polychromatic light.

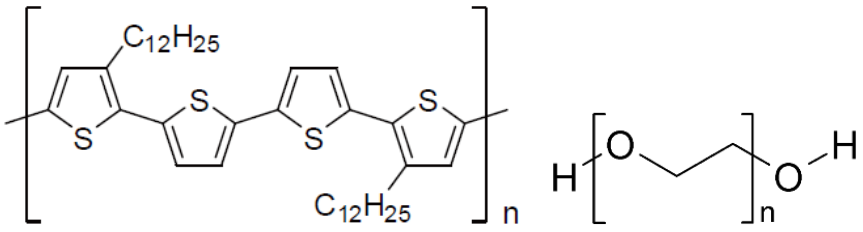

Scheme 2.1. Molecular structure of poly(3,3‴-didodecylquarterthiophene) (PQT-12) and poly(ethylene oxide) (PEO)

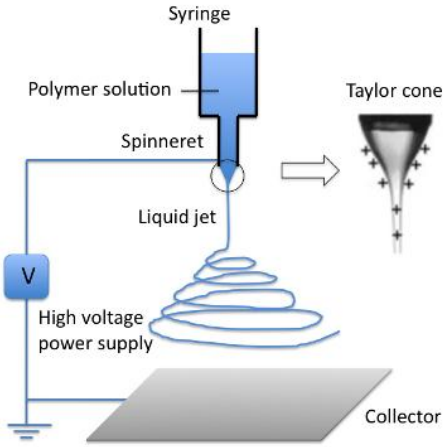

Figure 2.1. Schematic diagram of electrospinning process.

III. Results and Discussion

3.1 Fabrication of PET-textile OFETs

The textile-based OFET devices in BGBC structure were fabricated on the highly flexible plain woven PET textile consisting of 40-μm-thick PET fibers with 60-μm-wide empty space between the fibers (Figure 2.2). Overall fabrication process of textile-based OFET device is described in Figure 2.3. We introduced the buffering layer over the textile by using cured PDMS to fill the empty space and flatten the pristine textile for the preparation of other components of the transistor device. The Au electrode with Cr as adhesion layer was deposited on the PDMS-buffered substrate by thermal evaporation using the shadow mask for the formation of the patterned gate electrode. PDMS thin film was chosen as the gate dielectric due to its intrinsic elasticity and high mechanical strength.[6] The cured PDMS film on the OTS-treated SiO_2/Si wafer was transferred onto the textile substrate.[7] The capacitance of 1-μm-thick PDMS dielectric was about 1.05 nF cm^{-2}. As the source and drain electrodes, 40-μm-thick gold electrode was thermally evaporated through the shadow mask. The cross-sectional SEM image depicted in Figure 2.4 shows the well-established structure of the textile-based devices with PQT-12-based nanofibers without any defects.

We prepared organic semiconducting nanofibers by electrospinning method. There are several reasons why we selected electrospinning method for the deposition of semiconducting nanomaterial. Firstly, nanostructured organic materials are more favorable for the flexible electronics, especially in sensors, than thin films owing to their inherent flexibility, high-aspect-ratio, and unique photoresponsive property. Secondly, electrospinning is based on solution process and gives a number of nano-sized active channels from the small amount of the solution. Thirdly, electrospun nanofibers can be easily aligned by using the collector rotating at a proper speed.[8] Finally, direct solution process on PDMS dielectric layer is not preferred because the solvent can be swelled in PDMS destroying the original shape.[9]

PQT-12, the well-known p-type semiconducting polymer with high field-effect mobility and air stability, was utilized as the active material for charge transport.[10] In general, the conjugated polymers are hard to be electrospun from the pure solution due to their low solubility, low molecular weight, rigid backbone and high crystallinity that can cause the blockage of the nozzle.[5b] Therefore, the well-spinable polymer, PEO, with high molecular weight was added in the PQT-12 solution as supporting polymer for continuous production of electrospun nanofibers. Blending the semiconducting polymers and the supporting polymers in a solution is one of the well-known method for electrospinning semiconducting nanofibers.[11] The results from the optical microscope image in bright field exhibit the well-aligned PQT-12:PEO nanofibers while overall reddish color of nanofibers shown in the dark-field image indicates the high uniformity and crystallinity (Figure 2.5). From the result of SEM analysis, we could observe

slightly rough surface of nanofibers demonstrating the morphology determined by the composition of PQT-12 and PEO. The average diameter of PQT-12:PEO nanofibers was about 800 nm.

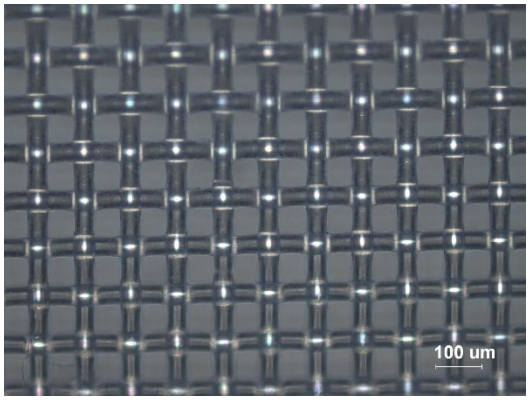

Figure 2.2. OM image of pristine PET textile (×100)

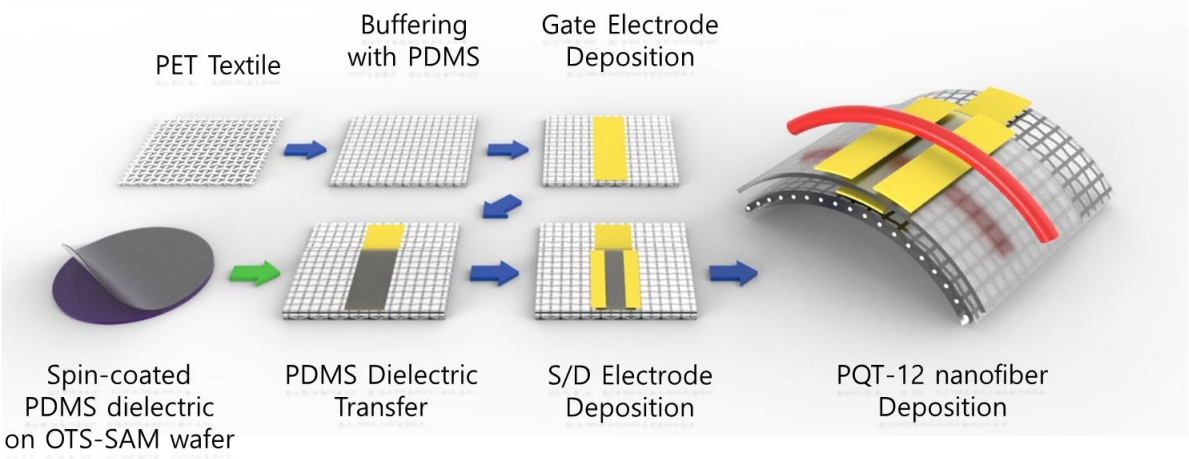

Figure 2.3. The fabrication process of textile-based OFETs.

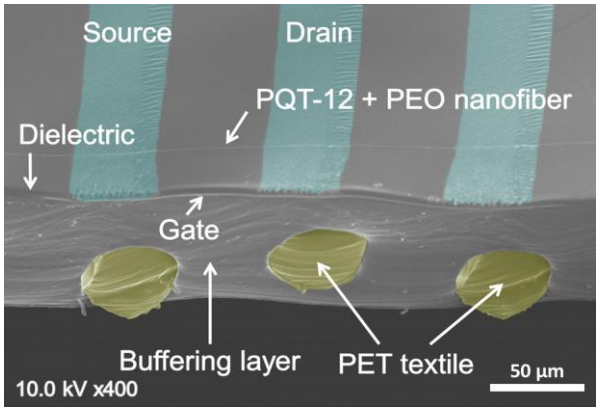

Figure 2.4. Cross-sectional SEM image of textile-based OFETs

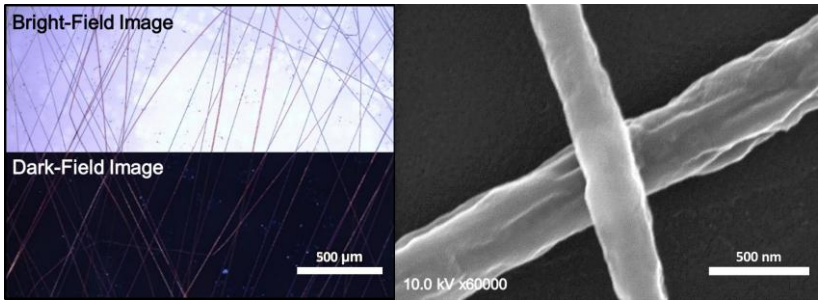

Figure 2.5. OM images of PQT-12:PEO NFs on bright-field (left, above) and dark-field (left, below), and SEM image of PQT-12:PEO NFs (right).

3.2 Electrical characteristics of textile-based OFETs

We determined the electrical characteristics of PQT-12:PEO nanofibers on the conventional OTS-treated SiO_2/Si substrate with BGBC geometry as shown in Figure S2.1. Three nanofibers showed 2.25×10^{-2} $cm^2V^{-1}s^{-1}$ of maximum hole mobility and 1.95×10^3 of on/off ratio in N_2 atmosphere (W/L = 1.504, saturation regime). The lower performance compared to the thin-film transistor can be affected by PEO acting as the trap sites for the efficient charge transport. In addition, this result is considered as underestimated because of narrow channel width with regard to the rounded surface of nanofibers and unfavorable contact between the rigid SiO_2 dielectric layer and the rough surface of PQT-12:PEO nanofibers.

To explore the electrical property of PQT-12:PEO nanofibers with maximum contact area between dielectric and nanofibers, we fabricated the coplanar-gate transistors using ion-gel dielectric with high capacitance of 10 μF cm^{-2} (Figure S2.2.). The highest mobility in linear regime were obtained as 112 $cm^2V^{-1}s^{-1}$ with 5.93×10^3 of on/off ratio (W/L = 0.06). It is well known that ion-gel dielectric can result in the remarkable performance due to the increased charge carrier density and filling of trap sites. However, the mobility in this configuration is also a bit overestimated value caused by the penetration of ions into the active layer by the Coulombic interaction between charges and ions.[12]

Finally, the current-voltage characteristics of the textile-based OFETs with PQT-12:PEO nanofibers were measured as shown in Figure 2.6. Transfer and output graph of the typical textile-based OFETs represents 2.96×10^{-3} $cm^2V^{-1}s^{-1}$ as maximum mobility in N_2 atmosphere (on/off ratio = 1.86×10^3). In ambient condition, they showed slightly reduced performance influenced by oxygen and moisture. ($\mu_{h,max}$: ~7.35×10^{-4} $cm^2V^{-1}s^{-1}$, I_{on}/I_{off}: ~10^2) The relatively less field-effect mobility of textile-based OFETs is attributed to the relatively longer channel length (50 μm) than that (4 ~ 10 μm) of the conventional silicon-wafer-based devices due to the more trap sites in the charge transporting channel despite the reduced contact resistance between the elastic dielectric layer and the active layer.

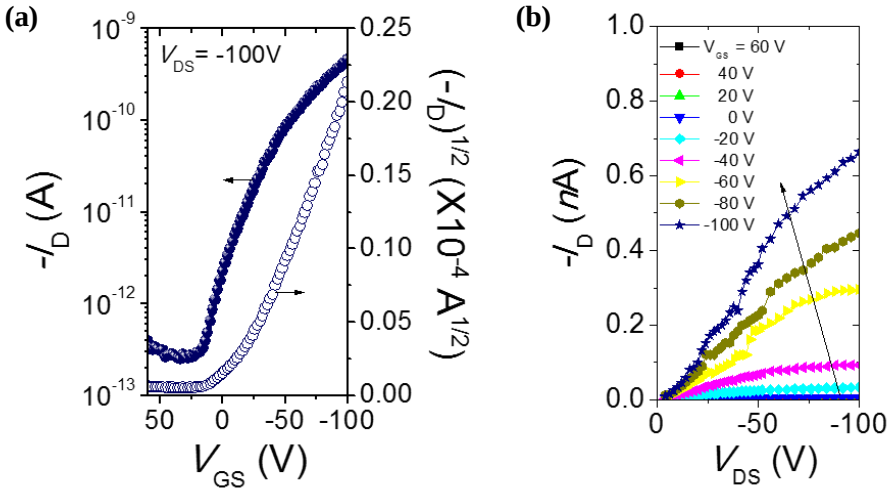

Figure 2.6. Electrical characteristics of textile-based OFETs; a) Transfer and b) Output characteristics.

3.3 Mechanical Stability

To confirm the potential for use in wearable electronic devices, we demonstrated the mechanical stability test of textile-based OFETs composed of flexible components. The bending test at various cylinder-like stages with six different bending radii, 6.7, 4.6, 3.5, 2.7, 1.6, and 0.75 mm, was performed as depicted in Figure 2.7, 2.8. Intriguingly, the textile-based OFET devices exhibited the stable electrical performance under extremely small bending radius of sub-millimeter scale up to 0.75 mm. Furthermore, after the bending test, they showed the consistent electrical property in recovered status with the initial status.

To substantiate the reproducibility of textile-based OFET device, bending cycle test was conducted by measuring the current-voltage characteristics every 100 cycles up to 1000 cycles at bending radius of 2.5 mm. From the bending test over 1000 cycles, we could observe the constant levels of on-current and off-current attained from transfer graph, giving noticeable mechanical stability in OFET performances. (Figure 2.9, 2.10)

The mechanical stability of the devices with different types of substrate was investigated as comparative test to verify the efficiency of textile substrate for flexible OFETs. We introduced the PET film substrate and PDMS-only substrate to the OFET devices fabricated in identical process except for the preparation of the PDMS-buffered PET textile. We measured the electrical characteristics of the devices with film-type substrate and PDMS-only substrate under the same bending test with previously performed in textile-based OFETs up to bending radius of 0.75 mm, as shown in Figure 2.11 and Table 2.1. In comparison to the report in 2012, the mechanical stability of OFETs on polyimide (PI) substrates were remained under the bending radius of ~1.27 mm which is extremely small but slightly higher value than that of our result.[13]

As a result, our PET textile OFET platform showed the outstanding features in the nearly constant on-current of 90.5 %, compared to PET film substrate (40.5 %) and PDMS-only substrate broken down at bending radius of 3.5 mm. The reason of serious decrease of on-current of OFETs on PET film substrate is that components of the devices were damaged due to the rigid surface of the film. In the case of OFETs based on PDMS-only substrate, their shape was easily deformed leading to the severe rupture of the device, especially to the electrode. This results suggest the importance of combination of the PET textile framework and elastic component to obtain mechanical strength as well as high flexibility. In this regard, PDMS-buffered PET textile is considered to be fairly suitable for the substrate for flexible OFET devices.

Table 2.1. Summary of relative decrease of on current (%) of PET textile, PET film, and PDMS-only substrate under different bending radius.

Bending Radius [mm]	Relative Decrease of On Current [%]		
	PET Textile	PET Film	PDMS-only
Initial	100.0	100.0	100.0
6.7	108.5	80.2	71.9
4.6	104.9	76.3	84.0
3.5	102.7	66.1	Broken down
2.7	98.8	58.0	-
1.6	92.4	48.2	-
0.75	92.4	38.9	-
Recovered	90.5	40.5	-

Figure 2.7. Typical photographic image of textile-based OFET upon bending at radius of 0.75 mm.

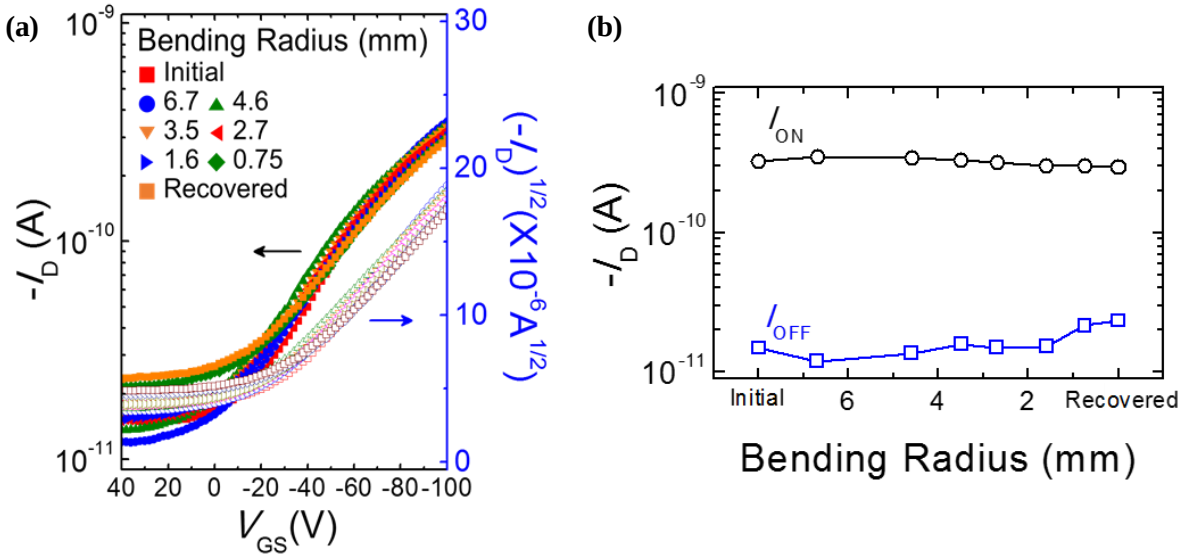

Figure 2.8. a) Transfer characteristics under different bending radii (6.7, 4.6, 3.5, 2.7, 1.6, 0.75 mm) and b) change in on-current and off-current under various bending radius.

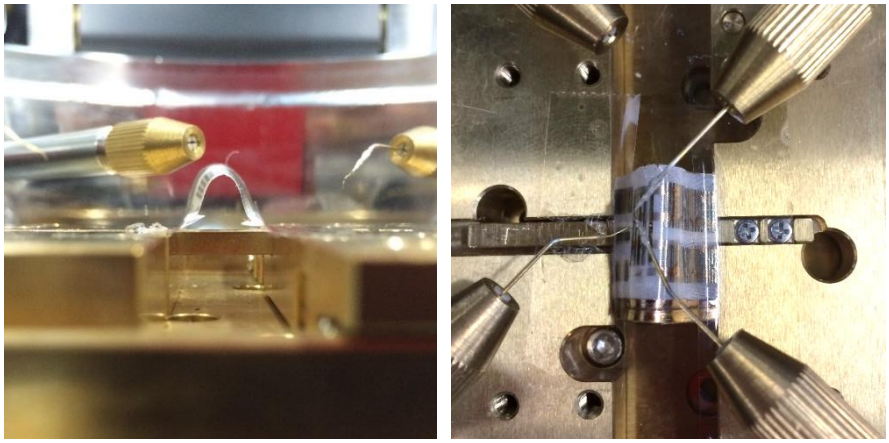

Figure 2.9. Photographic image of textile-based OFET upon bending cycle test.

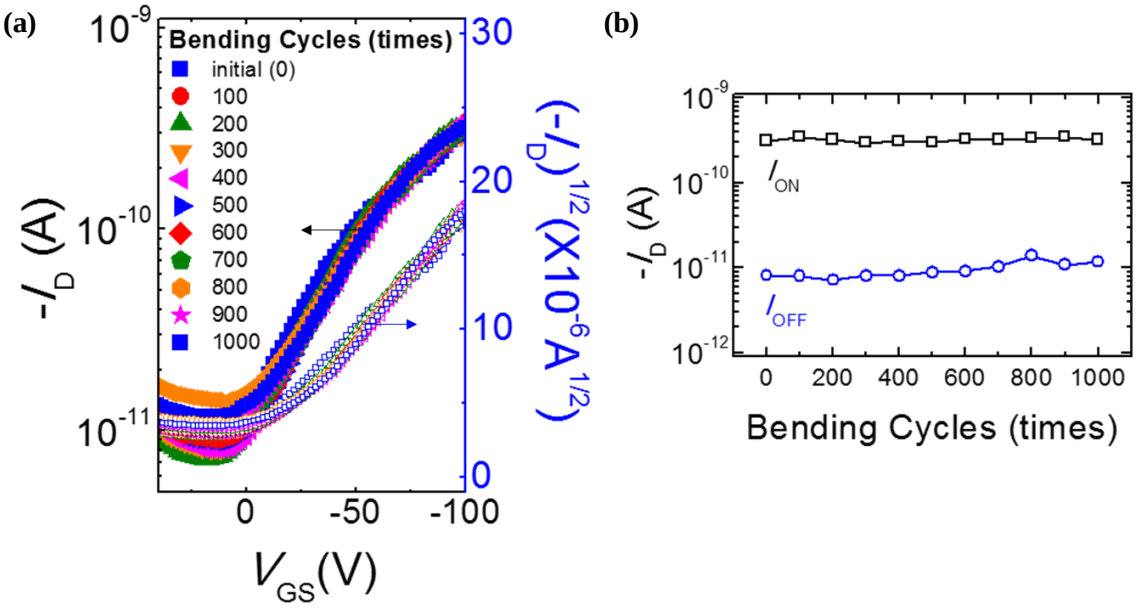

Figure 2.10. a) Transfer characteristics and b) change in on-current and off-current upon bending cycle test (up to 1000 cycles) with bending radius of 2.5 mm.

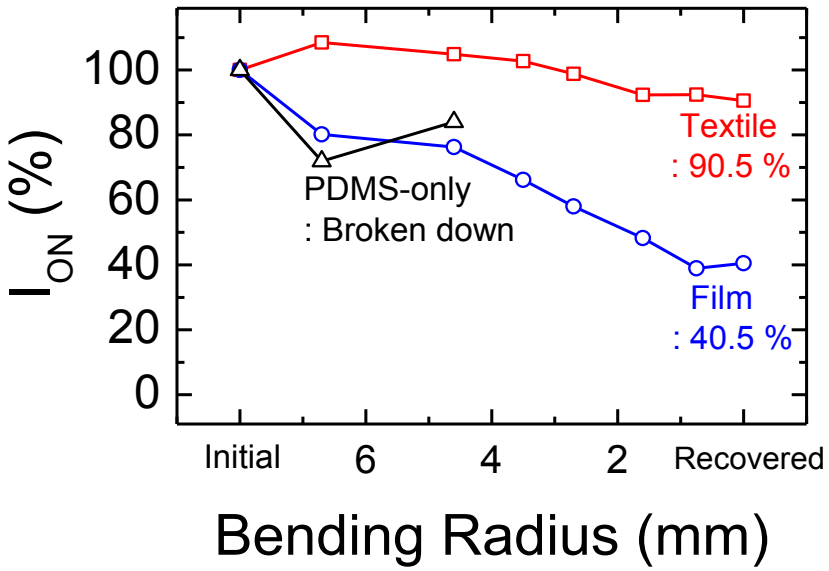

Figure 2.11. Comparison of change in on-current under various bending radii with OFETs based on PET film substrate and PDMS-only substrate

3.4 Optoelectronic characteristics

As shown in Figure 2.12. and Table 2.2, the absorption spectra of PQT-12:PEO solution and thin-film gives the value of the wavelength at maximum absorption peak (λ_{max}) at 470 nm and 535 nm, respectively, which are consistent with λ_{max} of pure PQT-12 solution and thin film. In other words, the optical property of the PQT-12 in the composite was not influenced by PEO at all. λ_{max} of nanofibers was observed at 585 nm, slightly red-shifted from that of thin film indicating the enhanced crystallinity of PQT-12 in nanofibers.[14] It is noted that the semiconducting polymer in the nanofiber can exhibit more ordered molecular packing with regard to previously reported aligned chain orientation of polymer with stretched backbone during the electrospinning process.[15] The high crystalline structure of organic semiconductors can facilitate the photoconductivity.

We characterized the optoelectronic properties of textile-based device based on PQT-12:PEO nanofibers with photoresponsivity in ambient atmosphere. Electrical characteristics were measured in dark condition, monochromatic laser sources with the fixed intensity of 100 μW cm^{-2} at different wavelengths (470, 535, 585, 670 nm) and polychromatic light source with intensity of 6 mW cm^{-2}. (Figure 2.13) The device showed significantly increased on-current under the exposure of the light at wavelength below 585 nm which is λ_{max} of PQT-12:PEO nanofibers, compared to the on-current values under the dark condition and the irradiated light at 470 nm. We could observe the substantial increment of both on-current and off-current under the polychromatic light source with high intensity. These results can be considered to develop the potential application of textile-based OFET devices to flexible photosensors with high sensitivity.

Table 2.2. Summary of maximum absorption wavelength (λ_{max}) of PQT-12-only, PQT-12+PEO solution in chlorobenzene, spin-coated PQT-12-only, PQT-12+PEO thin-film, PQT-12:PEO single nanofibers

Sample Type		λ_{max} **[nm]**
Solution (Chlorobenzene)	PQT-12-only	**470**
	PQT-12+PEO	**470**
Thin-Film (Spin-coating)	PQT-12-only	500, **535**, 570
	PQT-12+PEO	500, **535**, 570
Single Nanofibers (Electrospinning)	PQT-12:PEO	545, **585**

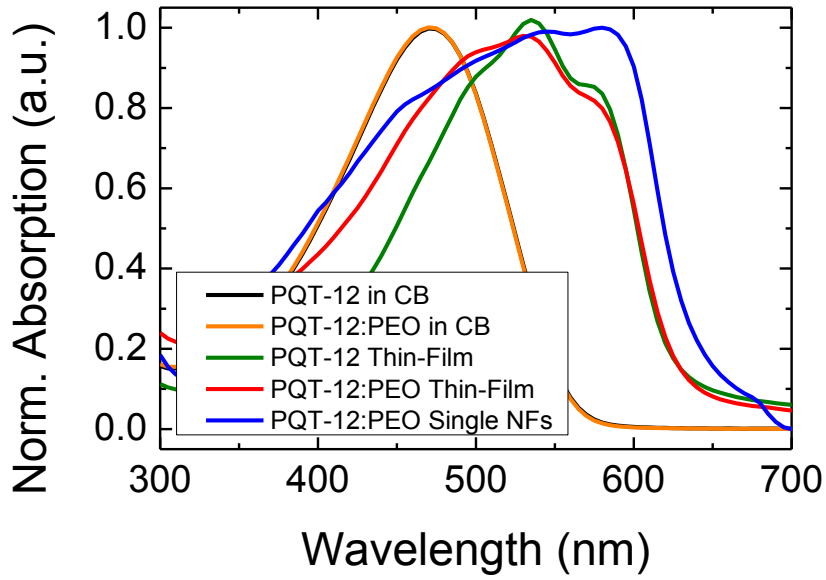

Figure 2.12. UV–vis spectra of PQT-only, PQT-12:PEO solution in chlorobenzene and spin-coated PQT-only, PQT-12:PEO thin-film, and PQT-12:PEO NFs.

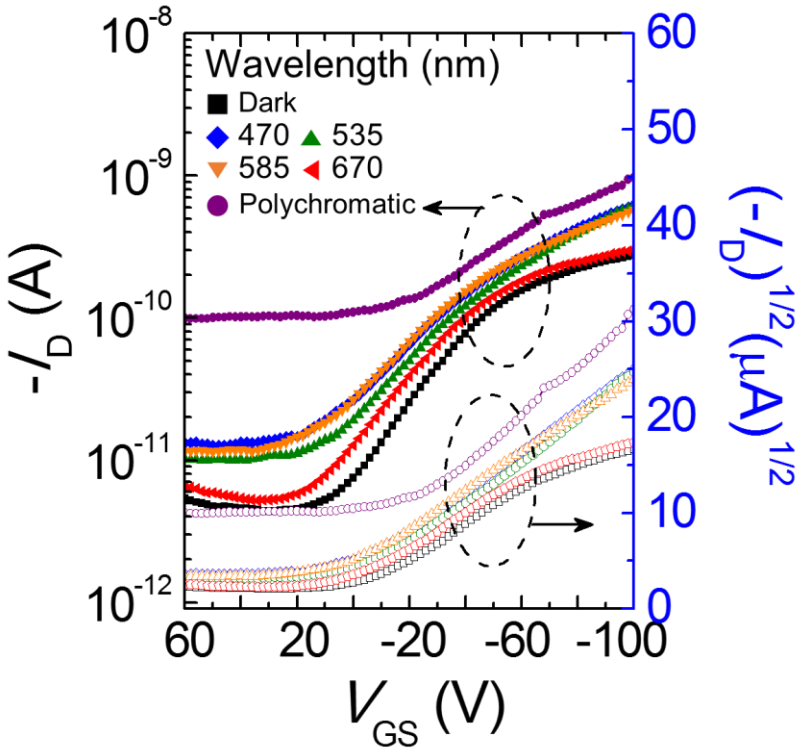

Figure 2.13. Transfer characteristics of textile-based OFETs under different light source.

3.5 Photosensor application

In accordance with the optoelectronic properties of textile-based OFET device involving PQT-12:PEO nanofibers, we performed real-time photo-sensing tests of the unit device. We measured the current signals by repeatedly turning on and off the light for several times at wavelengths of 670 nm and 470 nm, respectively. (Figure 2.14) Comparing with the result under the light at 670 nm, the irradiation of the light at 470 nm showed the higher increase in current signal as expected in previous experiment on optoelectronic characteristics.

Aiming to the realization of the image sensor for the practical application, the textile-based photosensor matrix was fabricated in 10×10 arrays of the unit devices. (Figure 2.15a) The device configuration and fabrication process are totally same with those of unit device. A hundred of the unit pixels were integrated by interconnection with word and bit lines. (2.5×2.5 cm^2) Each channel of the pixels possessed more than 10 semiconducting nanofibers. Consequently, the electrical properties of all pixels partially exposed to the polychromatic light source were expressed in two-dimensional (2-D) colored histogram depending on the variation of the on-current increment as shown in Figure 2.15b, c. The red colored pixels represent the light-exposed part of which the current is remarkably increased, while the blue area exhibits the region in dark condition. The reliability of the photosensor matrix suggests the possibility for the image sensor application with high sensitivity as well as flexibility.

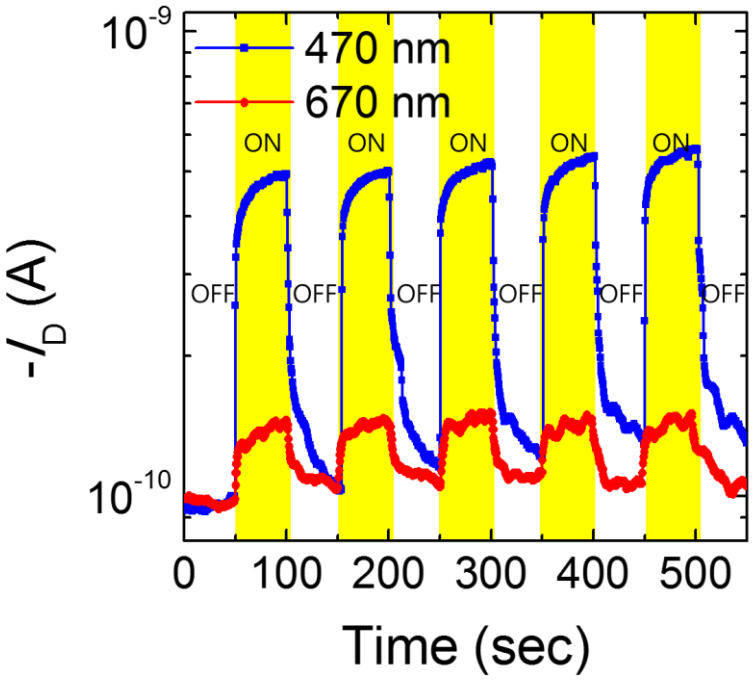

Figure 2.14. Real-time photo-sensing graph under 470 nm (blue) and 670 nm (red).

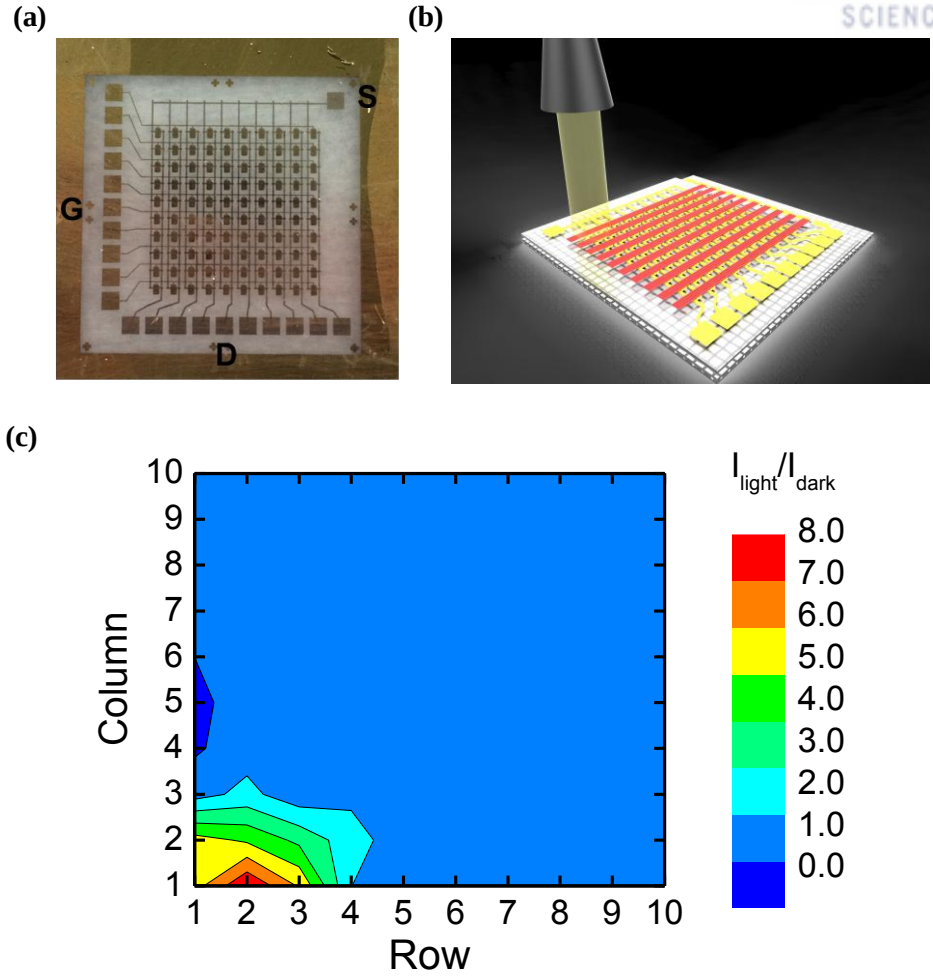

Figure 2.15. a) Photographic image of photosensing matrix (10×10) of the textile-based OFETs, and b) schematic illustration of sensor arrays partially exposed to the external light source. (intensity = 6 mW cm^{-2}) c) Spatial photosensing map of the textile-based photosensor matrix. The polychromatic light was positioned on (2, 1) of the matrix.

IV. Conclusion

In summary, we fabricated PET-textile-based OFETs with remarkable flexibility and mechanical robustness. The components of organic transistors were deposited on the PDMS-buffered textile substrate in the order of gate electrode, PDMS dielectric, S/D electrode and electrospun PQT-12:PEO nanofibers as the active channel. The textile-based OFETs showed reasonably high-performance electrical characteristics. ($\mu_{h,max}$ = 2.96×10^{-3} $cm^2V^{-1}s^{-1}$, I_{on}/I_{off} >10^3) Upon bending test at various radii (up to 0.75 mm), textile-based OFETs remained noticeably stable electrical performance compared to the OFETs based on PET film substrate and PDMS-only substrate, implying the noteworthy mechanical stability required for the ideal wearable electronic devices. The result of bending cycle test (~1000 cycles) represents the mechanical durability. In addition, the optoelectronic property was measured and maximum absorption wavelength of PQT-12:PEO NF was 585 nm. The textile-based OFETs could be utilized as photosensor by the increased on-current resulted from photogenerated charge carriers in PQT-12:PEO NFs. Eventually, the 10×10 arrays of photosensor matrix were fabricated and used as the image sensor with 2-D spatial response in the partial region exposed to the polychromatic light source. This research suggests this highly flexible textile-based OFETs as a strong candidate for the next-generation wearable photosensors or photoswitches.

V. References

1. (a) Murphy, A. R.; Fréchet, J. M. J., Organic Semiconducting Oligomers for Use in Thin Film Transistors. *Chemical Reviews* **2007,** *107* (4), 1066-1096; (b) Torsi, L.; Magliulo, M.; Manoli, K.; Palazzo, G., Organic field-effect transistor sensors: a tutorial review. *Chemical Society Reviews* **2013,** *42* (22), 8612-8628; (c) Schwartz, G.; Tee, B. C. K.; Mei, J. G.; Appleton, A. L.; Kim, D. H.; Wang, H. L.; Bao, Z., Flexible polymer transistors with high pressure sensitivity for application in electronic skin and health monitoring. *Nature Communications* **2013,** *4*.

2. Yi, H. T.; Payne, M. M.; Anthony, J. E.; Podzorov, V., Ultra-flexible solution-processed organic field-effect transistors. *Nat Commun* **2012,** *3*, 1259.

3. (a) Huang, J.; Zhu, H.; Chen, Y.; Preston, C.; Rohrbach, K.; Cumings, J.; Hu, L., Highly Transparent and Flexible Nanopaper Transistors. *ACS Nano* **2013,** *7* (3), 2106-2113; (b) Fujisaki, Y.; Koga, H.; Nakajima, Y.; Nakata, M.; Tsuji, H.; Yamamoto, T.; Kurita, T.; Nogi, M.; Shimidzu, N., Transparent Nanopaper-Based Flexible Organic Thin-Film Transistor Array. *Advanced Functional Materials* **2014,** *24* (12), 1657-1663; (c) Chortos, A.; Lim, J.; To, J. W. F.; Vosgueritchian, M.; Dusseault, T. J.; Kim, T.-H.; Hwang, S.; Bao, Z., Highly Stretchable Transistors Using a Microcracked Organic Semiconductor. *Advanced Materials* **2014,** *26* (25), 4253-4259; (d) Drack, M.; Graz, I.; Sekitani, T.; Someya, T.; Kaltenbrunner, M.; Bauer, S., An Imperceptible Plastic Electronic Wrap. *Advanced Materials* **2014**, n/a-n/a; (e) Lipomi, D. J.; Tee, B. C. K.; Vosgueritchian, M.; Bao, Z., Stretchable Organic Solar Cells. *Advanced Materials* **2011,** *23* (15), 1771-1775; (f) Müller, C.; Hamedi, M.; Karlsson, R.; Jansson, R.; Marcilla, R.; Hedhammar, M.; Inganäs, O., Woven Electrochemical Transistors on Silk Fibers. *Advanced Materials* **2011,** *23* (7), 898-901; (g) Lee, J. B.; Subramanian, V., Weave patterned organic transistors on fiber for E-textiles. *Electron Devices, IEEE Transactions on* **2005,** *52* (2), 269-275; (h) Fukuda, K.; Takeda, Y.; Yoshimura, Y.; Shiwaku, R.; Tran, L. T.; Sekine, T.; Mizukami, M.; Kumaki, D.; Tokito, S., Fully-printed high-performance organic thin-film transistors and circuitry on one-micron-thick polymer films. *Nat Commun* **2014,** *5*; (i) Kaltenbrunner, M.; Sekitani, T.; Reeder, J.; Yokota, T.; Kuribara, K.; Tokuhara, T.; Drack, M.; Schwodiauer, R.; Graz, I.; Bauer-Gogonea, S.; Bauer, S.; Someya, T., An ultra-lightweight design for imperceptible plastic electronics. *Nature* **2013,** *499* (7459), 458-463; (j) Ryu, G. S.; Jeong, S. H.; Park, B. C.; Park, B.; Song, C. K., Fabrication of organic thin film transistors on Polyethylene Terephthalate (PET) fabric substrates. *Organic Electronics* **2014,** *15* (7), 1672-1677.

4. Kim, W.; Kwon, S.; Lee, S.-M.; Kim, J. Y.; Han, Y.; Kim, E.; Choi, K. C.; Park, S.; Park, B.-C., Soft fabric-based flexible organic light-emitting diodes. *Organic Electronics* **2013,** *14* (11), 3007-3013.

5. (a) Yu, H.; Bao, Z.; Oh, J. H., High-Performance Phototransistors Based on Single-Crystalline n-Channel Organic Nanowires and Photogenerated Charge-Carrier Behaviors. *Advanced Functional Materials* **2013,** *23* (5), 629-639; (b) Luzio, A.; Canesi, E.; Bertarelli, C.; Caironi, M., Electrospun Polymer Fibers for Electronic Applications. *Materials* **2014,** *7* (2), 906-947.

6. Lötters, J. C.; Olthuis, W.; Veltink, P. H.; Bergveld, P., The mechanical properties of the rubber elastic polymer polydimethylsiloxane for sensor applications. *Journal of Micromechanics and Microengineering* **1997,** *7* (3), 145.

7. Sundar, V. C.; Zaumseil, J.; Podzorov, V.; Menard, E.; Willett, R. L.; Someya, T.; Gershenson, M. E.; Rogers, J. A., Elastomeric Transistor Stamps: Reversible Probing of Charge Transport in Organic Crystals. *Science* **2004,** *303* (5664), 1644-1646.

8. Teo, W. E.; Ramakrishna, S., A review on electrospinning design and nanofibre assemblies. *Nanotechnology* **2006,** *17* (14), R89.

9. Lee, J. N.; Park, C.; Whitesides, G. M., Solvent Compatibility of Poly(dimethylsiloxane)-Based Microfluidic Devices. *Analytical Chemistry* **2003,** *75* (23), 6544-6554.

10. Ong, B. S.; Wu, Y.; Liu, P.; Gardner, S., High-Performance Semiconducting Polythiophenes for Organic Thin-Film Transistors. *Journal of the American Chemical Society* **2004,** *126* (11), 3378-3379.

11. (a) Laforgue, A.; Robitaille, L., Fabrication of poly-3-hexylthiophene/polyethylene oxide nanofibers using electrospinning. *Synthetic Metals* **2008,** *158* (14), 577-584; (b) Lee, S.; Moon, G. D.; Jeong, U., Continuous production of uniform poly(3-hexylthiophene) (P3HT) nanofibers by electrospinning and their electrical properties. *Journal of Materials Chemistry* **2009,** *19* (6), 743-748; (c) Lee, S. W.; Lee, H. J.; Choi, J. H.; Koh, W. G.; Myoung, J. M.; Hur, J. H.; Park, J. J.; Cho, J. H.; Jeong, U., Periodic Array of Polyelectrolyte-Gated Organic Transistors from Electrospun Poly(3-hexylthiophene) Nanofibers. *Nano Letters* **2009,** *10* (1), 347-351; (d) Canesi, E. V.; Luzio, A.; Saglio, B.; Bianco, A.; Caironi, M.; Bertarelli, C., n-Type Semiconducting Polymer Fibers. *ACS Macro Letters* **2012,** *1* (3), 366-369; (e) Min, S.-Y.; Kim, T.-S.; Kim, B. J.; Cho, H.; Noh, Y.-Y.; Yang, H.; Cho, J. H.; Lee, T.-W., Large-scale organic nanowire lithography and electronics. *Nat Commun* **2013,** *4*, 1773.

12. Xia, Y.; Cho, J. H.; Lee, J.; Ruden, P. P.; Frisbie, C. D., Comparison of the Mobility–Carrier Density Relation in Polymer and Single-Crystal Organic Transistors Employing Vacuum and Liquid Gate Dielectrics. *Advanced Materials* **2009,** *21* (21), 2174-2179.

13. Wang, C.; Chien, J.-C.; Takei, K.; Takahashi, T.; Nah, J.; Niknejad, A. M.; Javey, A., Extremely Bendable, High-Performance Integrated Circuits Using Semiconducting Carbon Nanotube Networks for Digital, Analog, and Radio-Frequency Applications. *Nano Letters* **2012,** *12* (3), 1527-1533.

14. (a) Babel, A.; Li, D.; Xia, Y.; Jenekhe, S. A., Electrospun Nanofibers of Blends of Conjugated Polymers: Morphology, Optical Properties, and Field-Effect Transistors. *Macromolecules* **2005,** *38* (11), 4705-4711; (b) Chuangchote, S.; Sagawa, T.; Yoshikawa, S., Fabrication and Optical Properties of Electrospun Conductive Polymer Nanofibers from Blended Polymer Solution. *Japanese Journal of Applied Physics* **2008,** *47* (1S), 787.

15. (a) Bianco, A.; Iardino, G.; Manuelli, A.; Bertarelli, C.; Zerbi, G., Strong Orientation of Polymer Chains and Small Photochromic Molecules in Polyamide 6 Electrospun Fibers. *ChemPhysChem* **2007,** *8* (4), 510-514; (b) Fennessey, S. F.; Farris, R. J., Fabrication of aligned and molecularly oriented electrospun polyacrylonitrile nanofibers and the mechanical behavior of their twisted yarns. *Polymer* **2004,** *45* (12), 4217-4225; (c) Stephens, J. S.; Chase, D. B.; Rabolt, J. F., Effect of the Electrospinning Process on Polymer Crystallization Chain Conformation in Nylon-6 and Nylon-12. *Macromolecules* **2004,** *37* (3), 877-881.

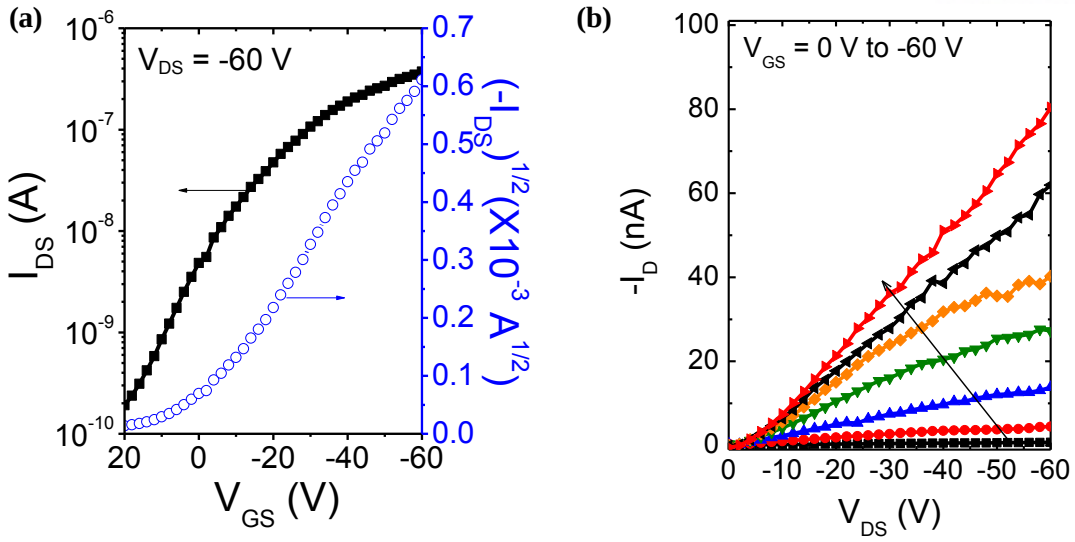

Figure S2.1. a) Transfer and b) Output characteristics of PQT-12:PEO nanofibers on OTS-treated SiO_2 (300 nm)/n-doped Si wafer with BGBC geometry.

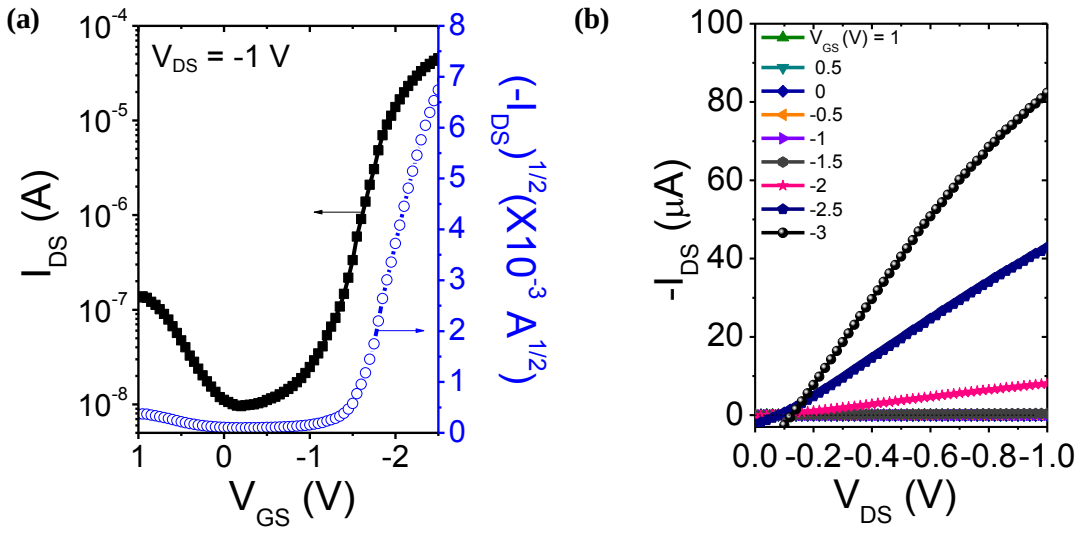

Figure S2.2. a) Transfer and b) Output characteristics of PQT-12:PEO nanofibers on coplanar-gate transistor based on ion-gel dielectric and polyimide (PI) substrate.

Acknowledgements (감사의 글)

UNIST에 학부생으로 입학하여 대학원 석사학위과정까지 어느덧 6년의 세월이 흘러 벌써 석사학위 졸업을 앞둔 시점이 되었습니다. UNIST가 개교하여 성장하는 모습을 지켜보며 저도 저 나름대로 공부도 하고 진로도 선택하여 지금은 연구자의 길을 걸어가고 있습니다. 돌아보면 그 동안 정말 많은 일이 있었던 것 같은데, 이 길을 흔들리지 않고 계속해서 걸어갈 수 있도록 도움을 준 모든 사람들께 감사 인사를 드리고 싶습니다.

학부생 시절부터 저를 지도해주시고 학부생 연구 프로그램 및 연구 인턴십을 거쳐 석사과정에 이르기까지 연구뿐 아니라 인생에 있어서도 아낌없는 조언과 격려를 해주시는 저의 지도교수님이신 오준학 교수님, 부족한 저를 잘 이끌어주셔서 정말 감사 드립니다. 학부생 때부터 지금까지 언제 뵈어도 늘 좋은 말씀 많이 해주시고 격려해 주시는 김병수 교수님, 양창덕 교수님, 정말 감사합니다. 또한 많이 바쁘신 와중에 저의 석사학위 심사를 맡아주신 모든 교수님들께 정말 감사 드립니다.

매일매일 얼굴 보며 한 공간에서 생활하는 가족과 같은 우리 SNDL 연구실 멤버들에게도 감사의 인사 전합니다. 선배로서 언제나 조언과 도움을 아끼지 않는 호정스틴 호정언니, 정글북 아름언니, 열정의 패셔니 문정언니, 씬스틸러 랩장 은광오빠 정말 감사합니다. 그리고 우리 동기들, 토마토 지형오빠, 열무 무열이, 지방대 골키퍼 윤호, 섬세한 동영이 잘 챙겨주어 고맙습니다. 우리 아래 기수들, 동갑내기 친구 해랑이, 그리고 인호와 철희에게도 고마움 전하고 싶습니다. 또한 지금은 군대에 있는 우리 동기 은엽이도 고맙습니다. 학부 인턴십 시절 야밤엔 언제나 함께였던 오 오랩사람들 무열, 유진, 다정언니 잊지 못할 추억 만들어줘서 고맙고, 그 든든함 덕분에 잘 버틸 수 있었던 것 같습니다.

저와 공동연구를 진행하며 많은 도움 주신 양창덕 교수님 연구실 김이호 차장님께도 감사의 말씀 전합니다. 공동연구를 진행하면서 2주마다 한번씩 미팅하며 많은 실험적 조언을 주신 KIMS 재료연구소 엄문광 박사님, 성동기 박사님, 이원오 박사님, 정병문 박사

님, 이제욱 박사님 및 모든 박사님들께 감사 드립니다.

학부시절부터 친구가 되어 마음을 나누며 수많은 추억을 쌓았고 또 언제나 힘이 되어 주는 동갑내기 친구들, 영원한 룸메이자 솔메 혜원이, 미국서부여행 동반자 부여고 순둥이 유진이, 유럽여행 함께한 은아, 우리 이쁜이들 모두 잘 되어서 기쁘고 정말 고맙다. 학부졸업 후에도 계속해서 즐거운 여행 함께하는 보급형 친구들도 늘 고마워. 대학시절 잊지 못할 추억이 된 지구방위대 친구들에게도 감사 인사 전하고 싶고, 앞으로도 축구면 축구, 연구면 연구, 일이면 일, 열심히 뛰고 승승장구하는 모습 뒤에서 지켜보며 응원할게.

항상 힘들 때마다 챙겨주고 멀리 있어도 안정을 찾을 수 있게 격려해주는 우리 부산여고 친구들, 쩡유니, 현가, 민지, 단비, 유주, 정말 너무나도 고마워. 앞으로 우리 하는 일 모두 잘 되었음 좋겠고 어떠한 일이 있어도 같이 울고 웃도록 하자. 더불어 중학교 시절 빼먹을 수 없는, 지금도 여전히 우정을 쌓고 있는 당리중 친구들과 서전학원 친구들에게도 고마움 전하고 싶다.

마지막으로, 이 세상에서 제일 사랑하는 우리 부모님과 하나뿐인 오빠에게 감사의 말씀을 전합니다. 저를 낳아주시고 사랑으로 길러주시어 제가 올바른 길로 나아갈 수 있도록 격려해 주시고 응원해주시는 우리 어머니, 아버지 언제나 사랑하고 감사합니다. 바쁜데도 항상 동생 챙겨주고 많이 생각해 주는 우리 오빠, 정말 고맙습니다.

모두에게 다시 한번 감사 드리며, 항상 감사하는 마음과 열정을 가지고 언제 어디서든 제게 주어진 것에 끊임없이 노력하는 자세로 임하겠습니다. 또한 매사에 충실하고 순간순간 최선을 다하는 사람이 되도록 하겠습니다. 감사합니다.